

Ecohydrologic Dynamics of Rock Moisture in a Montane Catchment of the Colorado Front Range

By

Ethan F. Burns

B.A., University of the South, 2016

A thesis submitted to the
Faculty of the Graduate School of the
University of Colorado in partial fulfillment
of the requirement for the degree of
Masters of Arts
Department of Geography
2022

Committee Members:

Holly Barnard

Katherine Lininger

Daniella Rempe

ABSTRACT

Burns, Ethan F. (M.A., Geography)

Ecohydrologic Dynamics of Rock Moisture in a Montane Catchment of the Colorado Front Range

Thesis directed by Associate Professor Holly R. Barnard

Warming across the western United States continues to reduce snowpack, shift melt dates, and increase atmospheric demand, leading to uncertainty about moisture availability in upland forest ecosystems. As many of these forests are characterized by thin soils and extensive rooting into weathered bedrock, deep vadose zone water is thought to be a central determinant in controlling late-season water availability and may mitigate water stress during a changing climate. A key impediment to understanding the role of the deep vadose zone as a reservoir lies in the challenge of quantifying the plant-available moisture held here and its relationship to snowmelt and rainfall timing. In this study, we quantify the spatiotemporal dynamics of rock moisture in a montane catchment of the Colorado Front Range. Direct measurements of rock moisture were accompanied by intensive monitoring of precipitation, transpiration, soil moisture, tree stress, and groundwater levels to elucidate the role of deep vadose zone moisture in sustaining transpiration and mitigating drought stress. Repeat NMR and neutron probe measurements in six boreholes spanning a catena of hillslope positions showed dynamic rock moisture is widespread. The magnitude of dynamic rock moisture change mirrors aboveground vegetation density, while the depth of dynamic water is confined to the uppermost weathered portions of the deep vadose zone (between the soil-saprolite interface and 5 m). Lower bound estimates of dynamic storage show weathered rock on southern aspects account for at least 9-12 % of the mean annual precipitation. Persistent

transpiration and discrepancies between estimated soil matric potentials and predawn leaf water potentials suggest rock moisture may mitigate drought stress. These findings provide some of the first direct measurements of rock moisture storage and use in the Rocky Mountains and support previous work that indicates rock moisture use is not just confined to periods of drought or to Mediterranean and semi-arid climates.

ACKNOWLEDGEMENTS

I would like to recognize the invaluable assistance of all those who were deeply involved in the completion of this research and my master's thesis. I am particularly thankful for my incredibly supportive advisor and committee (official and unofficial). Holly: your belief in my work and encouragement were invaluable. As were your soldering skills. Daniella: your excitement and energy were contagious, and your wordsmithing a godsend. Andy: While I literally could not have done this research without your unbelievable flexibility and willingness to loan out tools, I am most grateful for all the time and advice you shared with me over the long hours of NMR surveys. Logan: your clear explanations (and python script) were instrumental in my interpretation and understanding of the geophysical returns. Kamini: from zoom meetings to fieldwork, anytime I was around you I was learning. Katherine: thank you for your outside perspective and critical eye.

Thank you to all those who supported this work through funding, logistical support, or simple physical labor. I am grateful for the funding of this project through NSF Award #2012669. I can't say enough about Margaret, Brad, and the whole CU Radiation Safety Office. Thank you for helping me navigate regulations and for accommodating my early morning departures. I will forever be appreciative of all who helped lug heavy batteries, dig out the truck, climb trees, wake up for predawns, and get fieldwork done. Thank you, Alex, Sidney, Reece, Mykael, Luke, Matt, and many more! It was mostly fun.

I'm extremely grateful to all who inspired, supported, and encouraged me from near and far over the last few years. I am especially grateful to my family: Mom, Dad, SG, Seth, Joyce, Larry, Elizabeth, Margaret, and Helen. This was much easier knowing I had your support.

I'd like to thank my cohort, department, and those department-adjacent for creating a community for us here in boulder and keeping me sane.

Thank you Bran, Karen, Stephen, Martin, Kevin, and so many others at Sewanee.

You prepared me, inspired me, and helped me fall in love with understanding this beautiful world.

I am forever grateful.

Helen,

This journey would not have happened without you.

CONTENTS

SECTIONS

ABSTRACT	ii
ACKNOWLEDGEMENTS	iv
CONTENTS.....	vi
TABLES and FIGURES	viii
INTRODUCTION	1
MATERIALS and METHODS.....	3
Site Description.....	3
Borehole and Plot Descriptions	5
Precipitation	7
Quantifying Changes in Soil Moisture	8
Measuring Fluctuations in Groundwater	8
Estimating Plot Level Transpiration	9
Sapflow Sensor Installation	9
Error Correction and Conversion of Heat Flux to Sapflow	9
Scaling to the Plot Level.....	10
Predawn and Soil Matric Potentials.....	11
Quantifying Changes Rock Moisture.....	12
RESULTS	14
Meteorological Context	14
Soil Moisture.....	15
Groundwater	17
Plot Level Transpiration	20

Matric Potentials and Tree Stress	21
Comparing Transpiration, Soil Moisture and Matric Potentials	22
Quantifying Spatial and Temporal Distribution of Rock Moisture	23
Measurement Uncertainty and Error.....	26
Transpiration, Soil moisture, and Matric potentials.....	26
Rock Moisture and Groundwater.....	27
DISCUSSION	28
Rock Moisture Contributes to Transpiration in a Snow-Dominated Montane Ecosystem	28
Reductions in Rock Moisture Mirrors Vegetation Density and Subsurface Structure.....	30
Uptake of Rock Moisture May Mitigate Onset of Drought-Stress	32
Implications of Rock Moisture	33
COCLUSION.....	35
BIBLIOGRAPHY	36
SUPPLEMENTAL TABLES and FIGURES.....	43

TABLES and FIGURES

TABLES

1. Borehole and Plot Descriptions	6
S1. NMR and Neutron Probe Survey Dates.....	43

FIGURES

1. Map and Location of Gordon Gulch.....	4
2. Conceptual Cross Section or Hillslopes.....	6
3. Measured and Calculated Parameters Mid-S Plot	16
4. Measured and Calculated Parameters Lower-S Plot.....	17
5. Rock Moisture Surveys Show Gradual Drying	18
6. Groundwater levels for WY 2021	19
7. Comparisons of Water Potentials.....	22
8. Dynamic Rock Moisture as Measured by NMR.....	25
S1. Schematic of Dynamic Rock Moisture Calculation	43
S2. Measured and Calculated Parameters Upper-N Plot	44
S3. Measured and Calculated Parameters Lower-N Plot.....	45
S4. Correlation Between Transpiration and Diel Groundwater fluxes	46
S5. Comparisons of NMR and NP Surveys	47

INTRODUCTION

Transpiration is the dominant terrestrial flux in the hydrologic cycle and can account for more than two-thirds of total evapotranspiration in many upland catchments of the western United States (Alton et al., 2009; Jasechko et al., 2013; Li et al., 2019). Movement of this near-surface water has consequences for watershed processes including landscape evolution, carbon storage, streamflow, groundwater recharge, and nutrient cycling (Brantley et al., 2017). Describing and accurately quantifying the partitioning, storage, and flux of water from the root zone into the canopy is fundamental to our understanding of Earth-surface processes, crucial to accurately predicting ecosystem vulnerability to environmental change, and of great societal and scientific interest (Brooks et al., 2015). However, our knowledge of the spatiotemporal distribution of plant-available moisture storage and consequent uptake remains incomplete for many ecosystems and landscapes.

Historically, many studies of transpiration and root-zone water availability have focused on the soil where root density is often highest (Canadell et al., 1996; Schenk and Jackson, 2002). However, across many hillslopes of the mountain west, field observations indicate that soils are thin or nonexistent and are often underlain by thick envelopes of weathered, unsaturated rock (St. Clair et al., 2015; Leopold et al., 2013; Rempe and Dietrich, 2014; Wald et al., 2013). It has long been observed that woody plants often root into this weathered layer (Hellmers et al., 1955; Lewis and Burgy, 1964; Stone and Kalisz, 1991). In Mediterranean and semi-arid climates, plants may access moisture stored in this weathered rock (Rose et al., 2003; Salve et al., 2012; Zwieniecki and Newton, 1996). This “rock moisture” – similar in concept to soil moisture – refers to moisture held

above the water table but below the soil horizon in saprolite, sap rock, and/or fractured bedrock (Salve et al., 2012), and has been shown to account for as much as 27% of the total evapotranspiration in some instances (Rempe and Dietrich, 2018). Estimates of bedrock water-storage capacity can explain vegetation distribution (Hahm, Rempe, et al., 2019), as well as vulnerability to drought (Hahm, Dralle, et al., 2019; Hahm et al., 2020; McDowell et al., 2019). Rock moisture use has even been confirmed in locations with relatively shallow water tables (Hahm et al., 2020). Notably, a recent water-budget approach using remote sensing by McCormick et al. (2021) indicated that rock moisture use is not only widespread but likely the norm in many climatic, topographic, and ecological settings. As McCormick et al. (2021) suggest, rock moisture dynamics may be as important as soil moisture in understanding terrestrial water and carbon cycling as well as ecosystem response to environmental change.

Understanding rock moisture partitioning, storage, and use is particularly important in montane catchment ecosystems of the western United States. These catchments are critical sources of water for human use (Bales et al., 2006; Mote et al., 2005), serve as an increasingly important continental-scale carbon sink (Pacala et al., 2001; Schimel et al., 2002), and are home to millions of people living in the wildland-urban interface (Theobald and Romme, 2007). Montane forests are also among the most vulnerable to anthropogenic climate change (Beniston, 2003; Millar et al., 2007). Over the last 60+ years, warming has reduced snowpack, shifted snowmelt dates earlier into the spring (Harpold et al., 2012; Mote et al., 2005, 2018), and lengthened growing seasons. The implications of such shifts for montane ecosystems and downstream communities are notable. Snowmelt is a primary driver of groundwater recharge (Earman et al., 2006), streamflow (Berghuijs et al., 2014; Godsey et al., 2014), and forest productivity (Hu et al., 2010; Trujillo et

al., 2012). Given that rock moisture may serve as a buffer to moderate the impacts of climate change (Klos et al., 2018), this reservoir will likely impact how forests respond to longer growing seasons and shifts in precipitation regimes. While work in rain-dominated catchments has begun to elucidate the spatiotemporal dynamics of rock moisture use and storage (Hahm et al., 2020; Rempe and Dietrich, 2018), questions remain about the role rock water plays in sustaining transpiration or mitigating drought stress in upland snow-dominated catchments.

In this study, we investigate the ecohydrologic dynamics of rock moisture in weathered gneiss bedrock and its role in sustaining transpiration in an upper montane catchment of the Colorado Front Range. We ask: (1) Does rock moisture contribute to transpiration in this ecosystem? (2) How does the relative contribution of rock moisture to transpiration vary with respect to subsurface structure and vegetation density? (3) Might the uptake of rock moisture mediate drought-stress in upper montane tree species? We examine these questions through intensive monitoring of moisture storage and fluxes across one growing season. We utilize a suite of geophysical, tree physiological, and hydrologic instrumentation including; Nuclear Magnetic Resonance (NMR) and neutron probes, in situ soil moisture and sapflow sensors, meteorologic instrumentation, and groundwater pressure transducers.

MATERIALS and METHODS

Site Description:

Gordon Gulch is a 2.6 km², headwater catchment located at 2700 m in the upper montane zone of the Boulder Creek Watershed, Colorado, USA (40.028 N, 105.488 W) (Figure 1). Gordon Gulch and Boulder Creek are within the traditional territories of the Arapaho, Cheyenne, and Ute peoples

and until Euro-American colonization, served as critical winter camping territory (Crifasi, 2015). Post-colonization records of forest disturbance indicate a stand-replacing fire that burned in 1859 (Goldblum and Veblen, 2013). Stumps in the study area show sparse logging across the catchment in the 1930s and 1970s, while a 2004 fuels-reduction project created small clearings on portions of the north- and east-facing slopes (Figure 1).

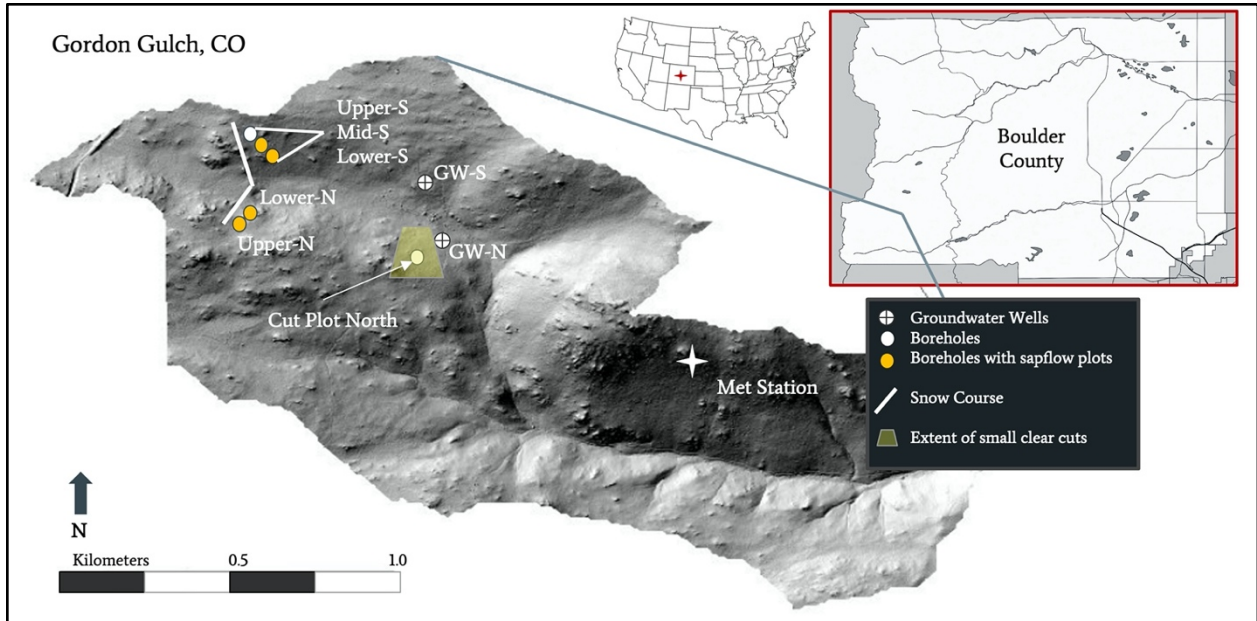


Figure 1. Digital elevation model (DEM) of Gordon Gulch with location of boreholes, groundwater wells, and meteorological station indicated. Mid-S, Lower-S, Upper-N, and Lower-N all have associated sapflow and soil moisture instrumentation. Circles with crosses indicate groundwater wells located on the hillslopes on both aspects. Yellow polygon indicates rough extent of thinning project near the Cut-Plot-N borehole. DEM and map modified from Warrell (2011).

A semi-arid catchment, Gordon Gulch receives an average of 527 mm yr⁻¹ of precipitation with peak precipitation arriving between April and June. Mean annual temperature is 5.3°C (data from PRISM Climate Group, 1980–2020) (<https://prism.oregonstate.edu/>). Like many Front Range catchments, aspect drives variability in energy balances, forest cover, and weathering. North-facing slopes retain continuous snowpack throughout the winter, whereas southern aspects display heterogeneous and transient snow. In the upper catchment where this study took place, mixed, ponderosa pine (*Pinus ponderosa*) and lodgepole pine (*Pinus contorta*) woodlands dominate

southern aspects with occasional stands of Douglas-fir (*Pseudotsuga menziesii*). Northern aspects are densely forested by lodgepole pine and minor amounts of Douglas-fir. Quaking aspen (*Populus tremuloides*) groves are found along the riparian zone at the catchment valley bottom.

Belowground, Gordon Gulch is underlain by thick envelopes of weathered sillimanite gneiss. Soils (mobile regolith) are typically thin (~0.4 m) with slightly thinner soils on south-facing hillslopes than on northern aspects. Depth to saprolite on north aspects along the valley bottom are much deeper with an average of 80 cm depth (Anderson et al., 2021). Below the soil layer, shallow seismic surveys by Befus et al. (2011) and St. Clair et al. (2015) indicate relatively uniform depths of weathering across both aspects in the uppermost reaches of Gordon Gulch. Saprolite extends to 4 m below the land surface while unweathered material is reached at roughly 15 m (Befus et al., 2011).

Borehole and Plot Descriptions:

Boreholes, drilled in 2014 and cased with PVC to one meter, provided access into the deep vadose zone. Three boreholes on the southern aspect, Upper-S, Mid-S, and Lower-S, span a range of hillslope positions, forest densities, and reach depths ranging from 5.6 to 9.7 m (Table 1). All three locations have thin soils (≈ 0.3 m) and saprolite extending down below the soil 2-4 m. The Upper-S plot consists of half lodgepole-pine forest and half open meadow while Mid-S is more densely forested with Douglas-fir, ponderosa pine, and lodgepole pine. Downslope, Lower-S contains a lower-density ponderosa pine and lodgepole woodland (Table 1, Figure 2).

Plot Descriptions								Species Count and Composition of Mature Trees						
Plot	Aspect	Landscape Position	Description	Soil Depth m	Borehole Depth m	BAI m ² ha ⁻¹	Transpiration mm m ⁻²	PICO	PIPO	PSME	Total	PICO %	PIPO %	PSME %
Upper-S	South	Upper slope	Half open meadow near road cut. *large PSME trees just outside plot	0.30±.04	5.6	1.64	NA	6	0	*0	6	100%	0%	*0%
Mid-S	South	Mid slope	Forested with understory and herbaceous ground cover	0.34±.04	9.7	3.09	32 ± 4.4	5	3	7	15	33%	20%	47%
Lower-S	South	Lower slope	Open ponderosa pine woodland. Grassy ground cover	0.30±.01	6.8	2.78	24 ± 2.9	2	12	0	14	14%	86%	0%
Upper-N	North	Upper slope	Dense lodgepole pine forest on rocky bench near ridge top. No to little understory	0.34±.05	1.5	4.05	31 ± 6.6	22	0	1	23	96%	0%	4%
Lower-N	North	Convergent toe slope	Dense lodgepole pine forest with standing dead, no to little understory	0.90±.1	2	2.78	20 ± 4.6	14	0	0	14	100%	0%	0%
Cut-Plot-N	North	Mid slope bench	Open cut for fire mitigation. Only small PICO saplings <4 cm DBH within 8 meters radius of well head. Mulched forest floor	0.30±.04	12	< 0.1	NA	10	0	0	10	100%	0%	0%

Table 1: Plot and borehole info. Yellow shading indicates plots with sapflow and soil moisture instrumentation.

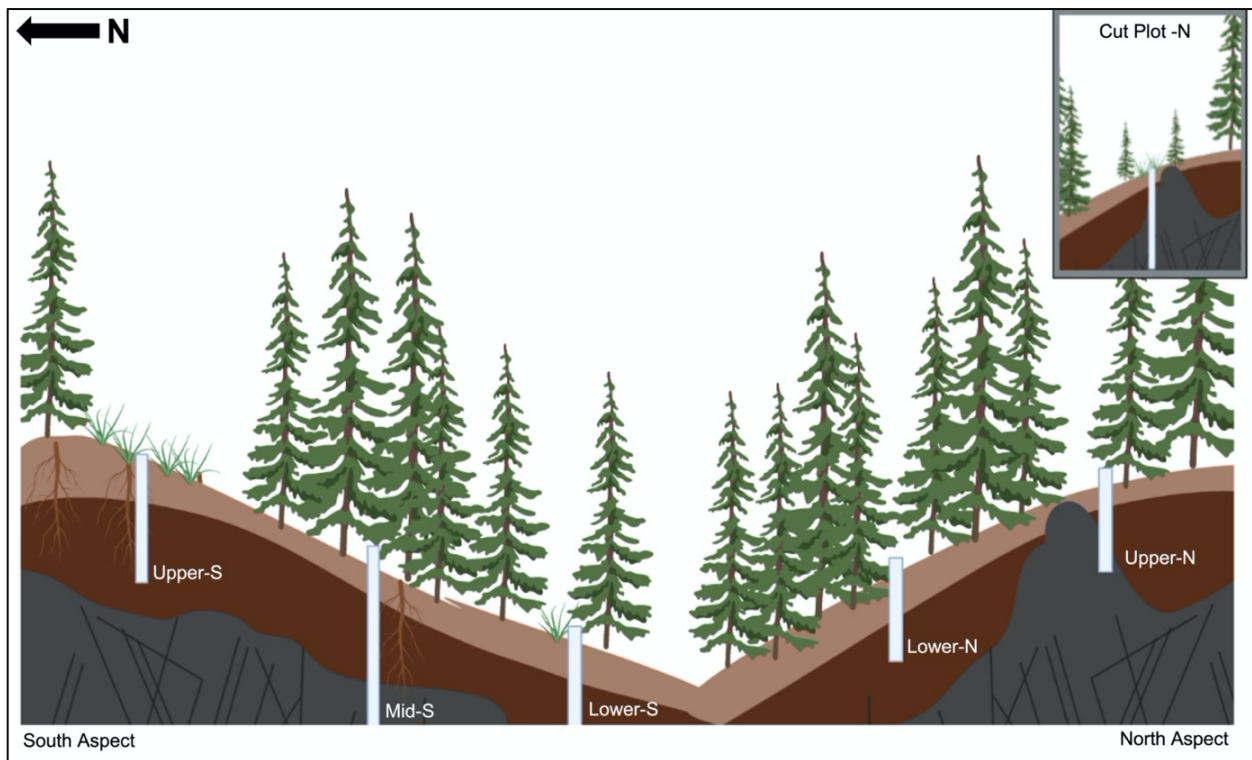


Figure 2: Conceptual cross section showing boreholes and landcover across both aspects. Boreholes and depths of soil and weathered rock are not to scale. North facing slopes are more densely forested with deeper soils in the lower hillslope position.

On the north aspect, one borehole drilled to ≈ 11 m in 2014 (Cut-Plot-N) and cased with PVC to one meter was used. However, as this borehole was located in a clear cut made in 2004 during a fuel-reduction treatment, we installed two new shallow boreholes (Upper-N and Lower-N) in fully forested locations. Drilled in March 2021, using a backpack-style drill (Shaw Tool of Yamhill, Oregon, USA), Upper-N is located near the ridge top where soil depth is similar to those found at Mid-S and Lower-S (Table 1). Upper-N is forested with lodgepole pine and few Douglas-fir. Unlike all other locations, Lower-N is in a convergent landscape position at the toe slope with relatively high-density lodgepole pine. Here, soils reach depths of roughly 0.9 m (Table 1). Four of the six boreholes, Mid-S, Lower-S, Upper-N, and Lower-N, were selected to house collocated sapflow and soil moisture plots. Sapflow and soil moisture sensors were not installed at the Upper-S and Cut-Plot-N boreholes as these locations had few mature trees large enough for sapflow sensors and were located at or near campsites where tampering was possible.

Precipitation:

Liquid precipitation data were collected continuously throughout the water year by a tipping-bucket rain gauge (TR-525m, Texas Electronics, Dallas, TX USA) at the south-facing Gordon Gulch Meteorological Station approximately (1.5 km) east and south of the study plots (Figure 1). Snow water equivalent (SWE) was measured approximately every 2-3 weeks between January and May using a federal-style sampler along a snow course paralleling the boreholes and sapflow plots. Samples were taken every 10 m, for 10 measurements per aspect.

Quantifying Changes in Soil Moisture:

Volumetric water content (θ_{soil}) was measured at Mid-S, Lower-S, Upper-N, and Lower-N, where sapflow was also measured. In plots Mid-S, Lower-S, and Upper-N sensors (HydraProbe, Stevens Water, Portland, OR USA) were installed at 10 cm and at 30 cm (typically within 5 cm of the soil-saprolite boundary). In the Lower-N plot, long-term sensors (CS616, Campbell Scientific, Logan, UT USA) installed in 2009 as part of the Critical Zone program were located in at 5, 50, 100, and 138 cm. Soil moisture was recorded every 15 minutes and averaged to calculate daily mean soil moisture. With sandy inorganic soils across the study site, HydraProbe sensors were set to the GEN calibration setting, the standard calibration for the US Department of Agriculture's SNOTEL and NOAA's Climate Reference Networks. Stevens Water reports accuracy in volumetric water content as $\pm 0.03(\text{m}^3 \text{ m}^{-3})$. Similarly, soil properties matched those required for the CS616 sensors to be left at the standard calibration (Diek et al., 2013). Campbell Scientific reports accuracy in volumetric water content as better than $\pm 0.025 (\text{m}^3 \text{ m}^{-3})$.

Measuring Fluctuations in Groundwater:

Diel fluctuations of groundwater have long been linked to transpiration (White, 1932). To determine if trees were likely sourcing moisture from the saturated zone, we analyzed water table data for diel fluctuation from the two groundwater wells (GW-S and GW-N) approximately 500 m downstream of instrumented sapflow plots (Figure 1). Groundwater levels were measured every 10 minutes using Solinst pressure transducers (Solinst Ltd., Georgetown, Ontario Canada) and corrected for changes in barometric pressure measured with Solinst Barologgers. Error in water table levels after correction for atmospheric pressure is ± 1 cm. To examine the correlations between transpiration and diel groundwater fluxes, we followed methods similar to those used

by Bond et al. (2002). Thirty-minute average sapflux data, created by averaging sapflux from six trees representing all three dominant species in the catchment, were paired with 30-minute groundwater table data. Correlations between timing of sapflux and water level height were analyzed separately for seven, 4 – 7-day time periods from June through September. For each period, the Pearson's correlation coefficient (r) between transpiration and groundwater level was calculated for at 30-min lag intervals (relating transpiration to progressively later time periods of groundwater levels) from 0 to 12 h. The presence of groundwater was checked for and measured manually in all boreholes every 2 weeks. Pressure transducers were not installed in any borehole as the majority remained dry throughout the study.

Estimating Plot Level Transpiration:

Sapflow Sensor Installation:

To estimate plot level transpiration, we scaled measurements of sapflow from the tree to the plot scale. One heat-ratio sapflow sensor (Burgess et al., 2001; Marshall, 1958) was installed on the western side of 8 trees per plot. Sapflow trees represented the species composition and size distribution of mature trees in the plot (Table 1). Sapflow was measured at two depths: 1 cm and 2.5 cm into the sapwood. For a description of installation see Kurpius et al. (2003). Data were recorded every 15 minutes with a datalogger and multiplexer in each plot (CR1000X and AM16/32b; Campbell Scientific, Logan UT, USA).

Error Correction and Conversion of Heat Flux to Sapflow:

Measured heat-pulse velocities were corrected for probe misalignment following Ambrose et al. (2010). When sensor failure created gaps in our data set, a linear relationship was used to fill data

gaps where strong correlation ($r^2 \geq 0.8$) existed between trees. Heat flux was converted into a sapflow velocity rate (cm hr^{-1}) using the Barrett et al. (1995) modified (Marshall, 1958) equation:

$$V_s = [V_h \rho_b (c_w + m_c c_s)] / \rho_s \times c_s$$

where ρ_b is the volumetric density of wood (kg cm^{-3}), c_w is the specific heat capacity of wood ($1200 \text{ J kg}^{-1} \text{ }^\circ\text{C}^{-1}$), c_s is the specific heat capacity of water ($4182 \text{ J kg}^{-1} \text{ }^\circ\text{C}^{-1}$), m_c is the volumetric water content of sapwood ($\text{cm}^3 \text{ cm}^{-3}$); and ρ_s is the density of water (0.001 kg cm^{-3}). Mean m_c and ρ_b were calculated from tree cores (at least three samples were taken per species per plot throughout the study period) from randomly selected trees co-located with sapflow plots. As we did not have measurements of wounding through time, we used the minimum wounding width of 2.0 mm (1.4 mm drill hole plus 0.3 mm on either side as indicated by Barrett et al. (1995) to select coefficients for the Burgess et al. (2001) polynomial correction. Thus, late-season corrected sapflow velocities are likely a conservative estimate of actual flow.

Scaling to the Plot Level:

To calculate sap flow volumetrically, we multiplied V_s by the corresponding sapwood area of the tree. Sapwood area for ponderosa pine and lodgepole pine was calculated from allometric relationships between diameter at breast height (DBH), or 1.3 m, and sapwood area derived from > 90 tree cores per species taken from across the catchment between 2013 and 2015. As no site-specific relationship between DBH and sapwood area existed for Douglas-fir, all Douglas-fir trees at each plot were cored at 1.3 m height after the summer field season to determine depth to heartwood. Because each thermocouple measured fluxes at two depths, the sapwood area of each

tree was divided into concentric rings such that each thermocouple defined the inner edge of a ring and provided a velocity for the sapflow in that area. The outer ring extended from the outer edge of the xylem to 1 cm deep while the inner ring reached from 1 cm to 2.5 cm deep. In trees where sapwood extended beyond the depth of our innermost sensor, a third ring was added between the inner sensor and the heartwood. We assumed a linear decline in sapflow from our innermost measurement to the heartwood boundary. Daily tree-level transpiration was then calculated by adding the volume of sapflow from each concentric circle. Sapflow was scaled to the plot level using species- and aspect-specific sapwood area to ground-area ratios following Pataki et al. (2000).

Predawn and Soil Matric Potentials:

To compare the decline in tree-available soil moisture with transpiration rates and tree moisture stress, we measured predawn leaf water potentials (Ψ_{predawn}) and calculated soil matric potentials (Ψ_{soil}). Predawn leaf water potentials were measured every 2-4 weeks throughout the study period with a Scholander-type pressure chamber (PMS, Corvallis, OR USA). During each survey measurements were taken between 0300 and 0430 from three to four trees at each sapflow plot and the mean leaf water potential reported. Water-potential values were corrected to ground level using the height at which the samples were collected and a gravitational gradient of 0.01 MPa m^{-1} . We estimated Ψ_{soil} from existing moisture release curves created from soils collected at 10 and 25 cm in Gordon Gulch in 2011 (Hinckley et al., 2014).

The wilting point of trees is often much lower than the “standard” wilting point or -1.5 MPa (Kramer and Boyer., 1995). Thus, to further aid in our interpretation of tree moisture stress, we

calculated the percent loss of conductivity (PLC) for a given species at a given location and time using species-specific vulnerability curves created by Piñol and Sala (2000). Domec et al. (2004) determined that the operating conductivity for Douglas-fir and ponderosa pine roots under moist conditions ranged between 20-30 and 30-45 PLC, respectively. We can expect at higher PLC values normal root function would become jeopardized (Domec et al., 2004). Thus, we classified PLC values over 30 as stressed. As others have shown drought-induced mortality is nearly ubiquitous across a range of taxa when embolisms lead to a loss of 60-80% of conducting xylem (Adams et al., 2017; Hammond et al., 2019), we conservatively classified values between 60% and 80% as extreme and values greater than 80% PLC as fully compromised.

Quantifying Changes Rock Moisture:

Rock moisture was measured with repeat nuclear magnetic resonance (NMR) and neutron probe surveys in all six boreholes. A total of seven NMR surveys were conducted with a Dart NMR Logging System (Vista Clara, Inc., Mukilteo, Washington, USA) every 2-4 weeks between May 20th and Sept 27th (Table S1). Measurements were taken at 0.25 m intervals for the first 3.5 m of depth and then at 0.5 m afterward. The volume of investigation is a shell, 0.23 m high, 1–2 mm thick, with a radius of 6.5–7.6 cm, centered around the vertical axis of the instrument (Walsh et al., 2013). Two recovery times were used (0.1 s and 1 s with 1000 and 100 stacks, respectively) for both transmit frequencies to maximize signal quality for short relaxation times. This acquisition scheme resulted in a total measurement duration of ~8 min at each depth interval. Data were processed using commercially available software (Javelin Pro Plus 4.6, Vista Clara, Inc.). Both frequencies were combined and a moving-window averaging filter was applied across four depth intervals (~1 m to 3 m depth and ~ 2 m below this) to increase the signal-to-noise ratio. Volumetric

water content, θ_{nmr} ($\text{m}^3 \text{m}^{-3}$), was taken as the value of the multiexponential fit at time zero. Noise level was calculated as the norm of the residuals after subtracting the multiexponential fit. The instrument was periodically checked in a water bath to confirm <1 % drift from the calibration.

Neutron probe surveys conducted approximately biweekly with a 503 Elite Hydroprobe (Instrotek, Concord, CA), ran from July 26th to September 14th. All neutron probe measurements began 0.25 m below the surface, lasted 32 s, and occurred at 0.25 m intervals to the bottom of the well or 7.25 m, whichever came first. The volume of investigation for neutron probes varies depending on water content. Generally, the measured water content (θ_{NP}) is the mean for a sphere measuring 30 cm across in wet material and 60–140 cm in dry material (Bell, 1987; Gardner, 1986). Relative to soils, a depth-by-depth calibration of neutron counts with water content was not feasible for the inaccessible, heterogeneous weathered bedrock at the site. While accurate measurements of absolute θ with a neutron probe are challenging, relative changes are more precise (Seyfried et al., 2001; Williams and Sinclair, 1981). Here, we report relative changes in θ_{NP} as calculated by a sand equivalent calibration created by Rempe and Dietrich (2018). Comparing overlapping NMR and neutron probe surveys provides greater confidence in the location and change in moisture content measured by late-season NMR surveys. Due to issues in shipping radioactive material, the neutron probe was not available for use at the study site until late July.

Uncertainty in both neutron probe and NMR measurement was estimated as the mean standard deviation of repeat measurements taken across the field season. Repeat neutron probe measurements were taken on the surface with the probe sitting on the case and at 3 m depth. Repeat NMR measurements were taken with the instrument resting at the bottom of boreholes Upper-S, Mid-S, and Cut-Plot-N, deep intervals that we assumed to have the minimum variation in water

content of all measurement locations. Uncertainty in changes in water content measured between early-season (wet) and late-season (dry) logs ($\Delta\theta_{\text{NMR}}$) was calculated using Gaussian error propagation. Uncertainty in depth of the measurement was estimated as 0.5 cm.

Dynamic rock moisture storage, $S_{\text{dynamic RM}}$ (mm m^{-2}), or stored water that is mobile either through extraction by woody vegetation or gravity driven drainage, was calculated as the season-long depth integral of $\Delta\theta_{\text{RM}}$. Assuming that the change in θ_{RM} occurred over the entire interval of sampling, the difference in θ_{RM} ($\text{m}^3 \text{m}^{-3}$) between wet-season (May 20th or June 2nd) and dry-season (Aug 17th or Sept 27th) surveys provides a season long $\Delta\theta_{\text{RM}}$, or $S_{\text{dynamic RM}}$ reported as a change in length per unit area (mm m^{-2}) (Figure S1). θ_{NMR} values taken at locations where the season-long $\Delta\theta_{\text{RM}}$ was less than uncertainty or while the zone of exploration was overlapping the soil horizon were removed and not included in $S_{\text{dynamic RM}}$ calculations.

RESULTS

Meteorological Context:

Water year 2021 was a wetter-than-average water year for Gordon Gulch with a drier-than-average late summer. The catchment received 625 mm of precipitation, 24% more than the 40-year annual mean of 527 mm. Much of this precipitation arrived in May and June when precipitation totals were 58% and 74% above the 40-year average respectively. Peak SWE, estimated to have occurred on April 24th, accounted for roughly 160 mm of the total precipitation on north-facing slopes but only 96 mm on southern aspects. Total precipitation for late summer (July-September) was 60% below average (114 mm).

Soil Moisture:

While initial θ_{soil} varied by plot, θ_{soil} was largely depleted in all shallow soil locations by the end of the water year (Figures 3, 4, and S2). In early June θ_{soil} at the Mid-S plot peaked at $0.18 \pm 0.03 \text{ m}^3 \text{ m}^{-3}$ at 30 cm. Moisture content at Lower-S and Upper-N peaked nearly a month later at $0.20 \pm 0.03 \text{ m}^3 \text{ m}^{-3}$. Moisture content in the soil layer then largely trended downward in all shallow soil locations, reaching $<0.07 \pm 0.03 \text{ m}^3 \text{ m}^{-3}$ at 30 cm by the end of the water year (Figures 3, 4, and S2). Soil moisture content at Mid-S was the lowest, $0.04 \pm 0.03 \text{ m}^3 \text{ m}^{-3}$ on Sept. 24th. By comparison, the north-facing, toe-slope plot, Lower-N, maintained higher θ_{soil} values throughout the study (Figure S3). At this site, θ_{soil} at 50 cm did not drop below $0.10 \pm 0.03 \text{ m}^3 \text{ m}^{-3}$ until mid-August while values at 100 cm remained above $0.18.0 \pm 0.03 \text{ m}^3 \text{ m}^{-3}$ throughout the study (Figure S3).

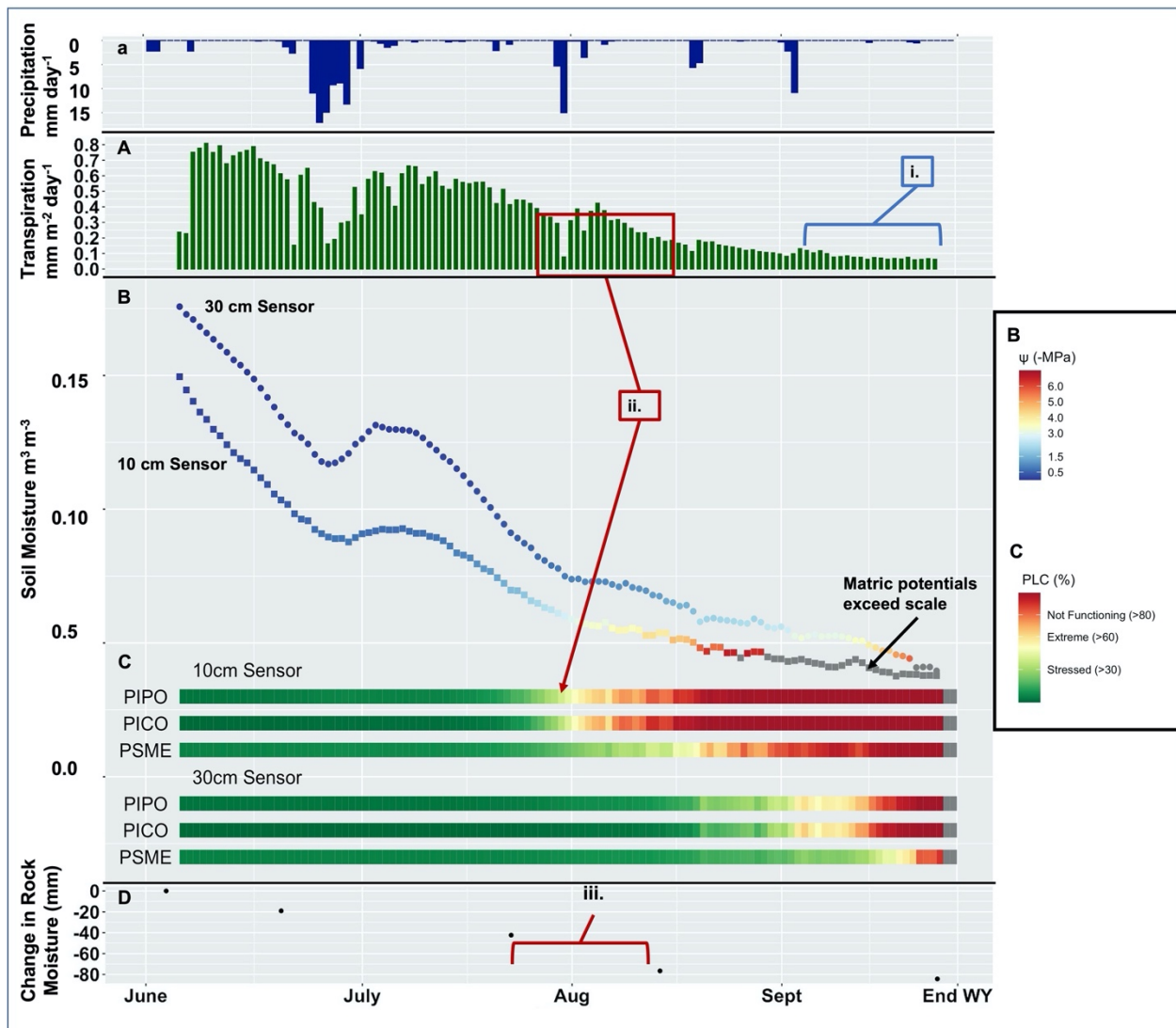


Figure 3: Measured and calculated parameters for Mid-S Plot. a) Precipitation. A) Plot level transpiration. B) Soil moisture with calculated matric potential overlaid in blue to red. C) Calculated Percent Loss in Conductivity (PLC) values in green to red bars. D) Change in rock moisture since the wettest survey on May 20th. i) Transpiration continues (A) even as soil matric potentials indicate soil moisture is not likely tree available (B). ii) Transpiration is still responsive to rain events (a and A) even as estimated PLC values suggest shallow roots should no longer function (C). iii) Greatest reductions in rock moisture (D) correspond with onset of low soil matric potentials and high PLC values at 10cm (C).

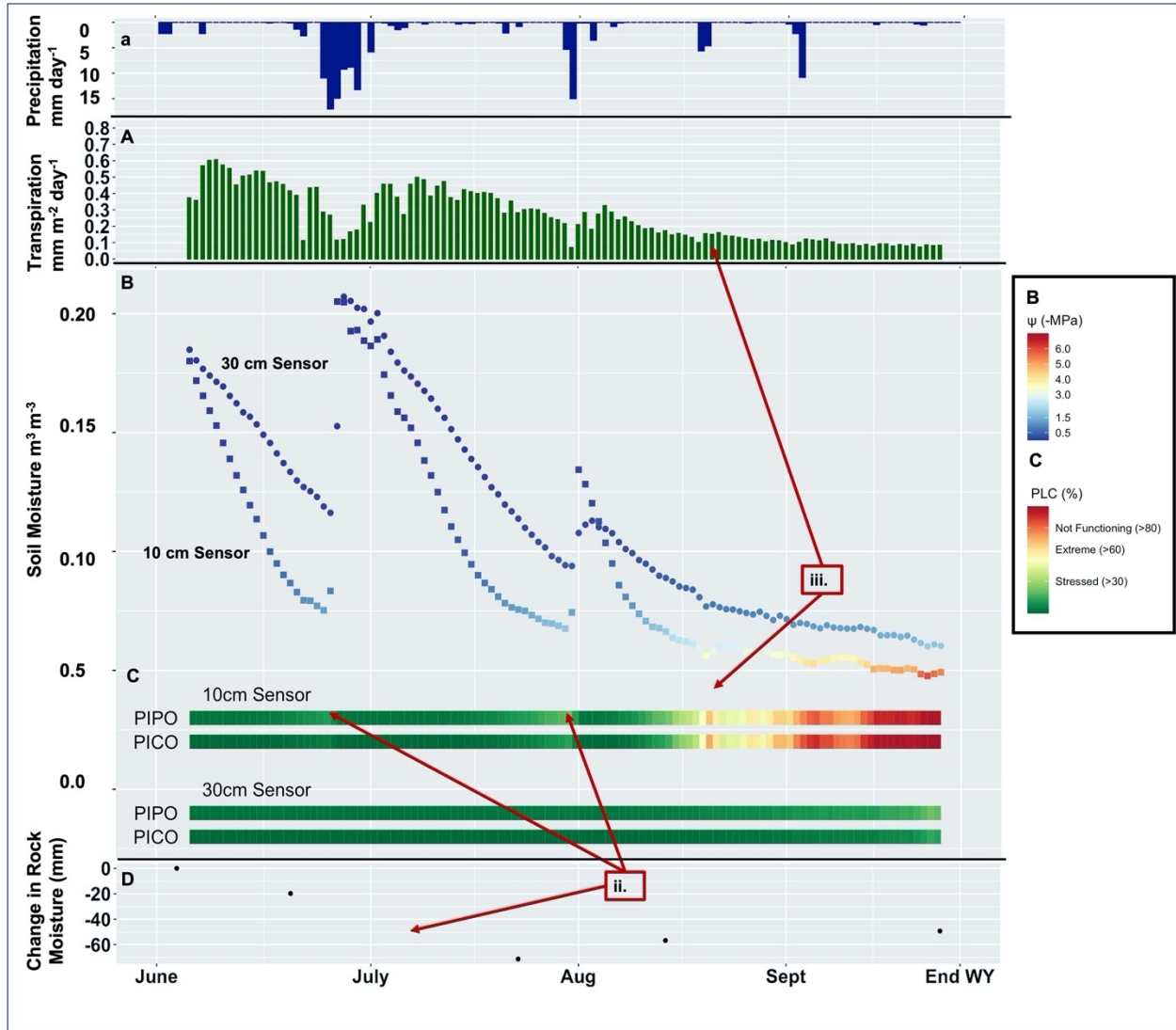


Figure 4: Measured and calculated parameters for Lower-S Plot. a) Precipitation. A) Plot level transpiration. B) Soil moisture with calculated matric potential overlaid in blue to red. C) Calculated Percent Loss in Conductivity (PLC) values in green to red bars. D) Change in rock moisture since the wettest survey on May 20th. ii) Greatest reductions in rock moisture occur (D) as shallow soils dry, matric potentials approach -1.5MPa (B), and roots become stressed (C). iii) Transpiration is still responsive to rain events (a and A) even as estimated PLC values suggest shallow roots should no longer function (C).

Groundwater:

Though some boreholes extended to nearly 11 meters, water was found in only two. In the shallow borehole at the Lower-N plot, water was found receding from 1.75 m to below the bottom of the borehole (2 meters below the surface) between May 20th and June 22nd. On the southern aspect,

water was found in the Mid-S borehole during the first three NMR surveys. Water levels in this borehole were measured at 8.1 m below the surface on May 20th, 8.5 m below on June 2nd and 8.35 m below the surface on June 22nd. The borehole was dry during and after the July 14th survey. Interestingly, repeat NMR surveys showed no variation in moisture content of the surrounding rock among surveys when water was found within the borehole and those when it was completely dry (Figure 5). Such an invariant rock moisture content suggests water held at this depth is confined to small fractures where the difference between field capacity and saturation is smaller than the margin of error for the instrument.

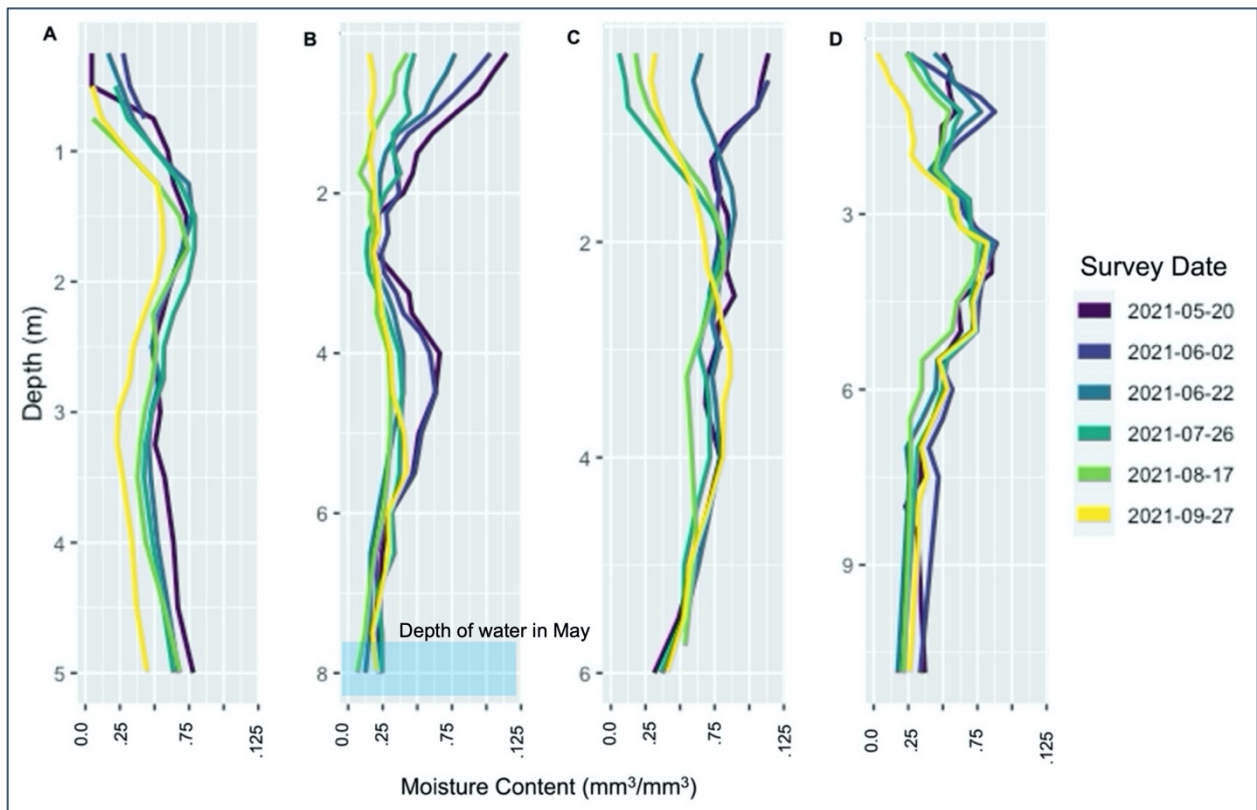


Figure 5: All repeat NMR surveys shown without associated error. A: Upper-S plot. B: Mid-S plot. C: Lower-S plot. D: Cut-Plot-N. Note gradual and progressive drying near the surface in all boreholes. Water was only found in the Mid-S plot. Water depths were measured manually three times at this location corresponding with the first three NMR surveys. Mid-S borehole was dry shortly after the June 22nd NMR survey. Depth to water in May is indicated with the blue shading above. Note no measurable change in moisture content at the bottom of Mid-S plot (B). This likely indicates water at this depth is held in small fractures (<2.3 mm across) where difference between saturation and field capacity is below the measurement error (see table S1 for calculations).

Downstream of the study site, water levels in the groundwater wells (GW-N and GW-S) showed both seasonal and daily fluctuations. Water levels in the GW-S peaked at 3.2 m below the surface on May 2nd before dropping to roughly 6 m below by the end of June (Figure 6). A small peak, following summer rain events, brought water levels back up to 5.5 m in July before levels began to drop for the remainder of the water year. By August, the water table was more than 6 m below the surface. Water levels in well GW-N rose from roughly 9.5 m below the surface in April to a peak of 8.25 m in early May. Water levels then rapidly fell, dropping below 9 m below the ground surface by June (Figure 6).

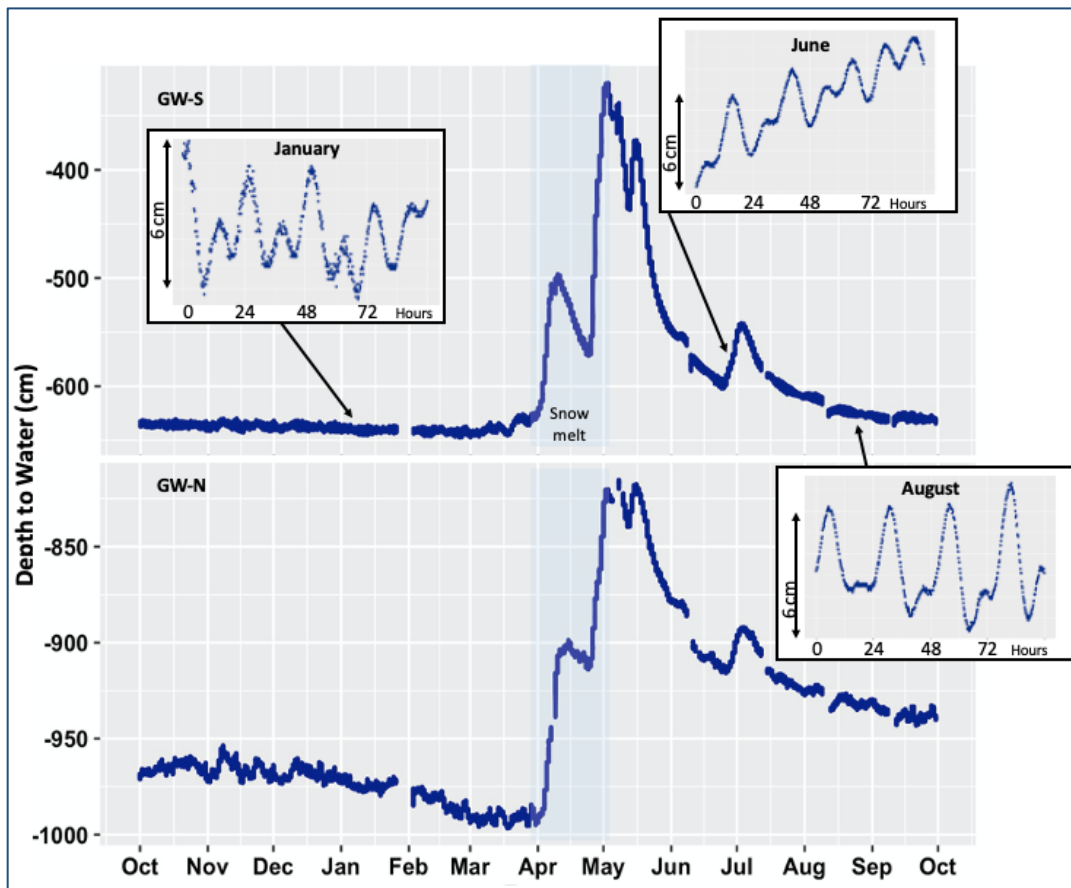


Figure 6: Groundwater levels for Water Year 2021 at the southern aspect well (GW-S) and northern aspect well (GW-N). Diel flux at both groundwater wells occurred during winter and summer months.

Water tables in both wells exhibited daily fluctuations during both summer and winter months. The magnitude of diel fluctuations averaged 5.3 and 3.6 cm per day in the south-facing and north-facing wells, respectively. In April and May, during the last snow melt, the diel signal “flattened” as water tables rose rapidly (Figure 6). Daily changes in water table height returned to pre-melt averages by early June. Correlations between transpiration and groundwater levels were weak ($r > -0.5$) throughout much of the growing season. Correlations only became stronger than -0.5 ($r = -0.57$, $p < 0.01$ and $r = -0.54$, $p < 0.01$) in GW-S and GW-N in early July and late September respectively with 0.5 and 6 hour lags (Figure S4).

Plot-Level Transpiration:

When comparing scaled transpiration rates (mm m^{-2}), similarly placed plots on opposing aspects transpired comparable amounts across the study period. Opposing upslope plots, Upper-N and Mid-S transpired 31 ± 6.6 and 32 ± 4.4 mm m^{-2} respectively, while their downslope counterparts Lower-S and Lower-N transpired 24 ± 2.9 and 20 ± 4.6 mm m^{-2} . Omitting dates with precipitation (and thus low VPD), south-facing plots exhibited higher early-season transpiration rates between $0.70 - 0.50$ $\text{mm m}^{-2} \text{d}^{-1}$ before declining rapidly to less than 0.1 $\text{mm m}^{-2} \text{d}^{-1}$ by the end of August (Figures 3 and 4). Transpiration rates in these south-facing plots (Mid-S and Lower-S) then remained relatively stable until the end of the study on September 24th. North-facing plots, on the other hand, showed lower early-season transpiration rates but more persistent late-season rates, rarely dropping below 0.1 $\text{mm m}^{-2} \text{d}^{-1}$ (Figures S2 and S3).

Matric Potentials and Tree Stress:

Mean Ψ_{predawn} at all plots ranged from -0.2 MPa in early June to -1.6 MPa by mid-September (Figure 7). While Mid-S exhibited slightly more negative values in May, for much of the summer plot averages were closely grouped with no clear distinction between aspect or landscape position. However, by late August, Lower-S showed greater stress, approaching -1.5 MPa while other plot averages did not exceed -1.0 MPa (Figure 7). The final Ψ_{predawn} measurements in mid-September at plots Mid-S, Lower-S and Upper-N (all shallow soiled locations) approached or exceeded -1.5 MPa while leaf-water potentials at Lower-N (a more deeply soiled location) remained < -1.0 MPa (Figure 7). Estimated 10-cm soil-matric potentials showed both south-facing plots crossing the -1.5 MPa threshold roughly one month earlier in late July to early August (Figure 7). Similar trends occurred at the soil-saprolite interface (30 cm) in plot Mid-S where estimated matric potentials dropped below -1.5 MPa in mid-August, eventually reaching values five times as negative as concurrently measured leaf water potentials (Figure 7A).

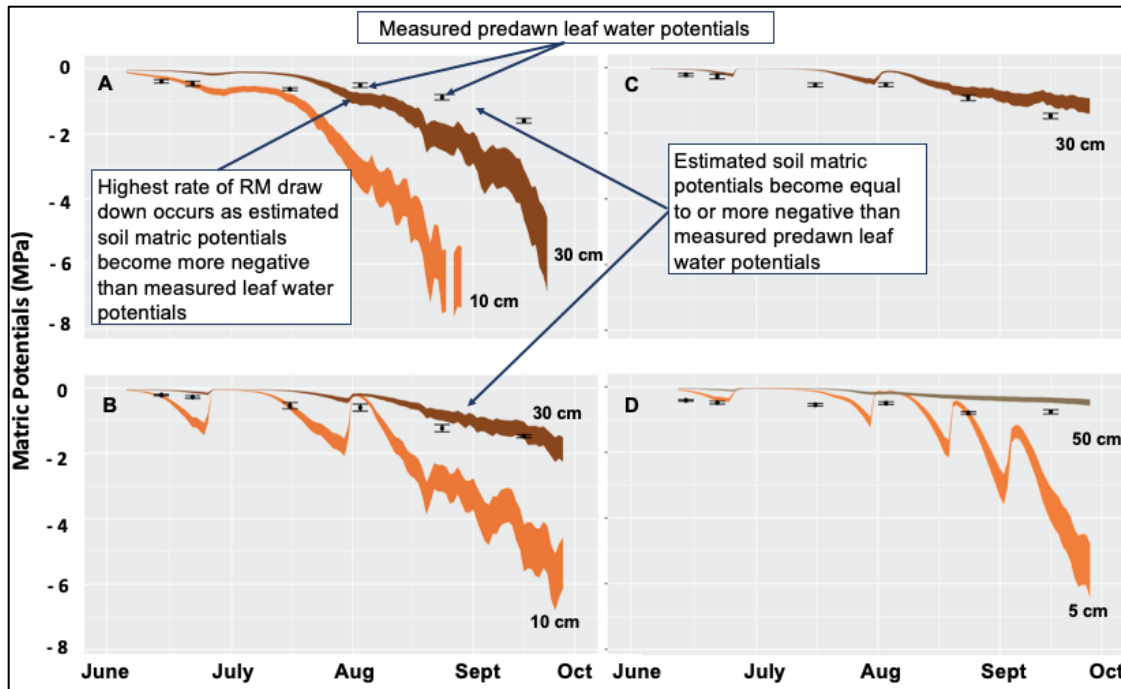


Figure 7: Comparisons between estimated soil matric potentials (orange and brown) and measured $\Psi_{predawn}$ (points with error bars) at: (A) Mid-S, (B) Lower-S, (C) Upper-N, (D) Lower-N. In both south-facing plots (A and B) measured leaf water potentials remain equal to or less negative than soil matric potentials at both 10 and 30 cm by the end of the study.

Estimated PLC for roots exceeded functional thresholds at both south-facing plots while remaining largely within functional thresholds on north-facing plots. By mid-August, PLC values for roots at 10 cm depth for all species in Mid-S and Lower-S plots exceeded the 60 % threshold. This same pattern occurred at 30 cm in the Mid-S plot by September. PLC values at 30 cm in the Lower-S and Upper-N plot remained at or below roughly 30 % throughout the study.

Comparing Transpiration, Soil Moisture and Matric Potentials:

Comparisons of plot-level transpiration alongside θ_{soil} , estimated Ψ_{soil} , estimated PLC values, and measured $\Psi_{predawn}$ show several important trends (Figures 3 and 4). Total transpired volumes at Mid-S were greater than those at Lower-S and comparable to those measured at Upper-N, despite having on average 28-35 % less volumetric water content at 30 cm than Lower-S and Upper-N

respectively. Late-season measured Ψ_{predawn} in all shallow soil locations were generally much less negative than estimated Ψ_{soil} at 10 cm and in some instances even less negative than matric potentials estimated for 30 cm. For example, at Mid-S estimated Ψ_{soil} at 30 cm, near the soil saprolite transition, reached -1.5 MPa by August 17th while measured Ψ_{predawn} did not cross the -1.5 MPa boundary until mid-September (Figure 7A). Similarly, during drying periods between rain events, estimated Ψ_{soil} at Lower-S were roughly equal to or more negative than measured leaf water potentials (Figure 7B). Transpiration rates increased in response to late-season rains, despite estimated PLC values suggesting shallow roots were fully compromised (PLC values >80%) on south-facing plots (Figures 3 and 4).

Quantifying Spatial and Temporal Distribution of Rock Moisture:

The vertical and temporal variability in dynamic rock moisture between and within boreholes was captured by both NMR and neutron probe surveys. After removing the first 0.5 m of measurements in each borehole to eliminate possible measurement of moisture held in the soil, dynamic rock moisture was observed in all boreholes that extended below the soil-saprolite interface, regardless of hillslope and land cover type.

Total storage (S_{total}) as measured by NMR down to 5 m ranged from 294 to 392 mm m⁻² or 57 to 93% of mean annual precipitation. Dynamic storage (S_{dynamic} mm m⁻²) ranged from 19 to 64 mm m² or 3.6 to 12% of annual precipitation (Figure 8). As neutron probe surveys were not calibrated to provide accurate volumetric estimates or rock moisture, we did not calculate S_{total} or S_{dynamic} for neutron probe. However, the direction and depth of measurable $\Delta\theta_{\text{np}}$ generally agreed with the season long trends of decreasing $\Delta\theta_{\text{nmr}}$. For example, while neutron probe surveys showed slightly

greater decreases in both the depth and volume of dynamic rock moisture, both methods indicated that dynamic moisture was concentrated between the soil-saprolite interface and a layer at approximately 2 - 2.5 m with stable, low-water contents (Figure S5). NMR showed measurable decreases below 2.5 m depth at only two boreholes, Upper-S and Mid-S, while no changes in rock moisture were observed by NMR below 5 m (Figure 8). Late-season neutron-probe surveys recorded very few decreases in rock moisture at depth as well. Only 3% of measurements below 3 m and <<1% (5 of 635 measurements) below 5 m showed any decrease in rock moisture. Such non-varying moisture contents suggest that no dynamic storage exists at depth, or that changes below 5 m were smaller than measurement uncertainty. Similarly, neither method showed an increase in rock moisture below 1.5 m suggesting little to no vertical drainage during the summer months (Figures 5 and S5). The few measurable increases in rock moisture that were observed near the surface occurred after summer storms at boreholes Upper-S, Lower-S, and Cut-Plot-N, locations with the lowest tree densities.

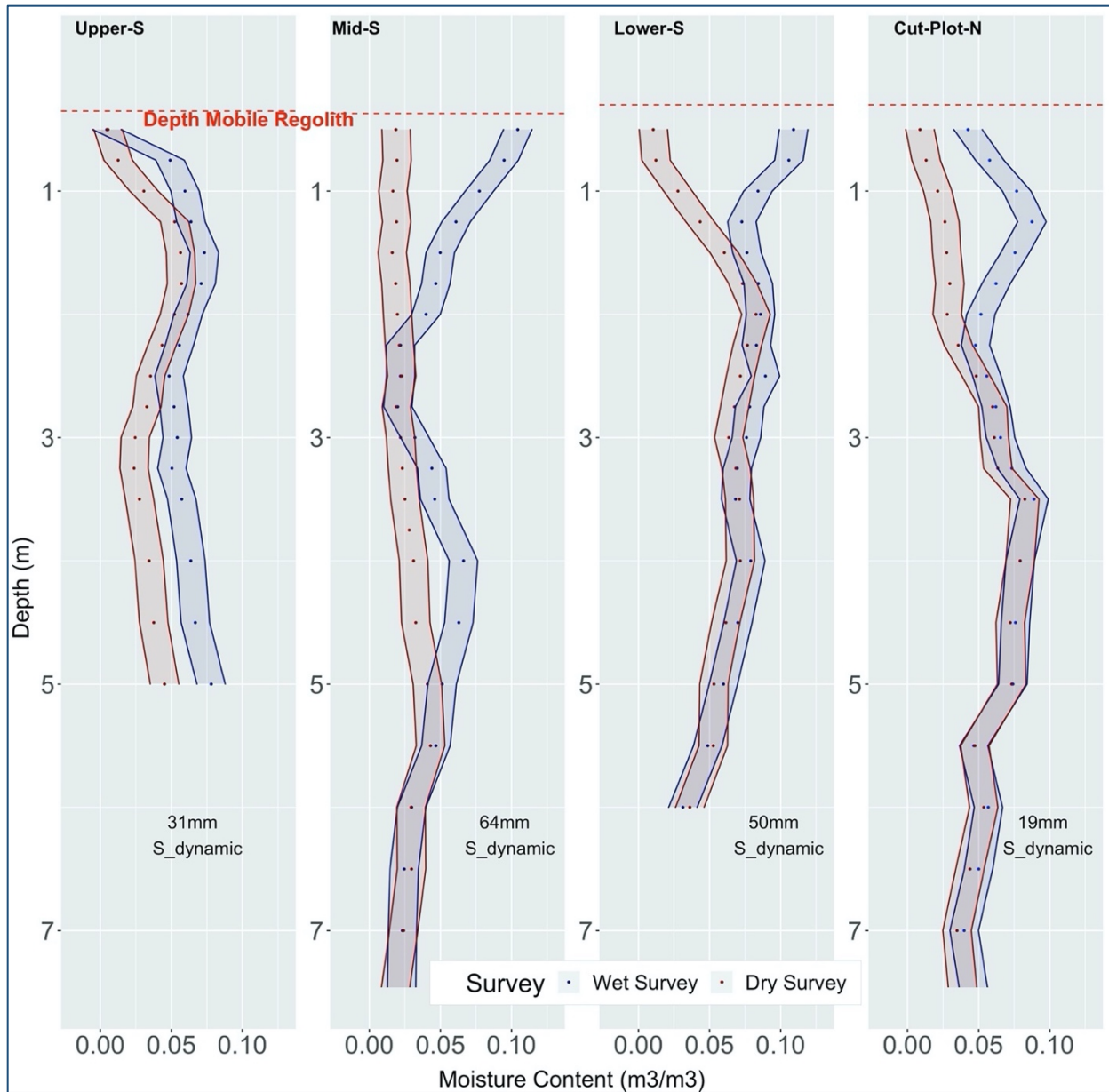


Figure 8: NMR surveys of all deep boreholes showing change in rock moisture. Dark blue represents the wettest survey (May 20th or June 2nd) while red indicates the driest survey (August 17th or September 27th). Shading indicates margin of error estimated from repeat measurements taken with the NMR probe sitting on the borehole bottom (see materials and methods for detail). Water was found in the Mid-S borehole during May and June. $S_{dynamic}$, the difference between wet and dry surveys where $\Delta\theta_{nmr} > \text{uncertainty}$, is reported for each well in mm m^{-2} .

The rate of change in rock moisture though time averaged between -0.5 mm d^{-1} at Mid-S, the most densely forested deep well location, to -0.2 mm d^{-1} at Cut-Plot-N, the most sparsely forested

location. Change in rock moisture at Mid-S and Lower-S began in June and increased to a peak of -1.06 and -1.19 mm d⁻¹ respectively before decreasing—and in the case of Lower-S, becoming positive (Figures 3D and 4D). Boreholes Upper-S and Cut-Plot-N (both sparsely forested locations) showed small increases in rock moisture at the near-surface in May and early June but did not show any measurable decrease in rock moisture until August and September. Shallow boreholes Upper-N and Lower-N, though not deep enough to provide estimates on rock moisture storage, did show reductions in moisture at the soil-saprolite interface (Figure S2 and S3). At the one measurement depth below the average soil depth, Upper-N exhibited a gradual reduction in soil moisture throughout the season (Figure S2). Measured moisture at Lower-N on the other hand varied between 8 and 10% volumetric water content until reaching a season low in September. Interestingly, this season low was the only variation in moisture content greater than uncertainty and occurred as roots in the uppermost layers of soil were becoming highly stressed (Figure S3). This mirrors, albeit to a lesser extent, the patterns seen on south-facing slopes where rock moisture draw down is greatest when roots at 10 cm experience potentially high rates of cavitation (Figures 3 and 4).

Measurement Uncertainty and Error:

Transpiration, Soil moisture, Matric potentials, and Groundwater:

Upscaling sapflow measurements creates numerous avenues for the introduction and propagation of error. Though we addressed possible error due to sensor misalignment, wounding, site-specific wood density, and moisture content (see materials and methods), various factors such as assumptions about even distribution of sapflow-conducting xylem introduced uncorrected and unmeasurable error. Here, reported error of plot-level transpiration represents sensor error ($\pm 8\%$)

(Steppe et al., 2010), uncertainty in sapwood area, and error introduced during scaling. Error of total transpired volumes for each plot ranged from 13-27 %. As others have noted, sapflow measurements can underestimate true sap flux density by as much as 35 % (Steppe et al., 2010). This factor, taken with our conservative method of correcting for wounding in which we provided only the minimum wounding width from sensor installation, suggests reported volumes likely represent a conservative estimation of daily and total transpiration. Uncertainty in the measurement of θ_{soil} was taken from manufacturer's reported values (see materials and methods).

Rock Moisture and Groundwater:

Repeat NMR and neutron probe surveys provided quality estimates of dynamic rock moisture storage and change in unsaturated weathered bedrock. Mean NMR noise levels were constant for all measurements at $0.012 \text{ m}^3 \text{ m}^{-3}$ (standard deviation $0.0051 \text{ m}^3 \text{ m}^{-3}$). In roughly 95 % of all measurements signal exceeded noise so that the signal-to-noise ratio was greater than 1. Uncertainty in rock moisture measurements from NMR (θ_{nmr}) and neutron probe (θ_{np}) surveys was estimated from repeat measurements at specific depths within each well. The standard deviation of all repeat θ_{nmr} ($n = 20$) ranged from 0.007 to $0.012 \text{ m}^3 \text{ m}^{-3}$, with a mean of $0.009 \text{ m}^3 \text{ m}^{-3}$. The mean standard deviation for repeat neutron probe measurements ($n = 113$) was 46 counts per 32 s, or approximately a $\Delta\theta$ of $0.003 \text{ m}^3 \text{ m}^{-3}$. Due to minor slipping and uneven well walls that occasionally caught probe centralizers, vertical uncertainty was estimated at 0.5 cm. Via the propagation of error, the uncertainty in $\Delta\theta_{\text{nmr}}$ and $\Delta\theta_{\text{np}}$ was then calculated at $0.01 \text{ m}^3 \text{ m}^{-3}$ and $0.006 \text{ m}^3 \text{ m}^{-3}$ respectively. As we lacked a material-specific neutron probe calibration, we could not directly compare θ_{nmr} and θ_{np} . However, survey dates where both methods were used show nearly a constant 2 to 1 relationship between methods with a linear relationship of $y=1.9x+0.17$ (r^2

= 0.51, $P < 0.01$). Uncertainty in the measurement of groundwater level was taken from manufacturer's reported values (see materials and methods)

DISCUSSION

Rock Moisture Contributes to Transpiration in Snow-Dominated Montane Ecosystem:

We found multiple lines of evidence that indicate transpiration drives reductions in rock moisture, especially in areas with shallow soils. Geophysical surveys showed moisture held in this weathered rock gradually declined throughout the growing season. In contrast, θ_{soil} in shallow-mantled locations rapidly diminished following snowmelt or summer storms while patterns in groundwater fluctuations were not closely tied to transpiration. Rock moisture depletion, $\Delta\theta_{\text{RM}}$, tended to begin at the soil-saprolite interface and progress downward throughout the entire dry season. The greatest reductions in rock moisture occurred in July and early August when transpiration rates remained relatively high, Ψ_{soil} approached -1.5 MPa, and groundwater levels were low. Repeat NMR surveys found no increase in θ_{RM} at depth > 1.5 m suggesting growing-season gravity drainage is minimal. We, therefore, hypothesize that the dynamic moisture observed across the catchment is primarily controlled by transpiration. Though smaller in magnitude in terms of both depth and volume of $S_{\text{dynamic RM}}$, this lack of vertical drainage and gradual drying match the patterns of rock moisture withdrawal reported by Rempe and Dietrich (2018).

Transpiration continued at plots where plant-available soil moisture was largely depleted. Estimated matric potentials at 10 cm on both south-facing plots exceeded -1.5 MPa (standard wilting point) on July 24th and by July 29th matric potentials fell to -2.0 MPa, which is at or below

the reported minimum growing season xylem matric potentials for Douglas-fir, ponderosa pine, and lodgepole pine (Piñol and Sala, 2000). Despite these very low potentials, transpiration rates continued steadily at around $0.1 \text{ mm m}^{-2} \text{ d}^{-1}$. Because the 30 cm sensors were located at the soil-saprolite interface and soil moisture increased with depth, we concluded soil moisture was no longer tree available at the mid-S plot and confined to only the deepest soils at the lower-S plot by early September.

The difference between estimated Ψ_{soil} and Ψ_{predawn} further suggests that the tree roots are accessing water beyond the soil matrix. Matric potentials in both south-facing plots at 30 cm became less than or equal to measured Ψ_{predawn} . At the mid-S plot, Ψ_{soil} was more than 5 times as negative than measured Ψ_{predawn} in early August before reaching -8.5 MPa by the end of the study. Predawn leaf water potentials have been shown to equilibrate with the most humid portion of the root zone, providing potential artificially high estimates of the matric potentials (Ameglio et al., 1999; Sucoff, 1972). While this propensity limits the ability of measured Ψ_{predawn} to accurately represent plant response to water stress, it suggests our observed differences between Ψ_{predawn} and estimate Ψ_{soil} are even greater. Thus, while the differences observed at the Mid-South plot suggests trees are accessing water from below the soil layer, trees in other shallow-soil locations where discrepancies between Ψ_{predawn} and estimate Ψ_{soil} are less, may be sourcing moisture from depth as well.

While daily fluctuations of groundwater were observed in both downstream groundwater wells, we found no evidence that these diel fluxes were driven by transpiration. Previous work examining diel fluctuations in ponderosa pine and Douglas-fir dominated landscapes have suggested trees are likely driving diel fluxes when correlations between groundwater or stream stage and transpiration

are strongly negative ($r \leq -0.70$) with shorter lags (≤ 4 hours) (Barnard et al., 2010; Bond et al., 2002; Graham et al., 2010; Harmon et al., 2020). Studies have also indicated that onset of diel fluctuations tend to correlate with the growing season and that the amplitude of groundwater fluxes increase when transpiration is high and hydrologic connectivity exists throughout the subsurface (Bond et al., 2002; Harmon et al., 2020). However, in Gordon Gulch, diel fluxes occurred throughout the entire calendar year, with no difference in the amplitude of fluctuations between winter months (Jan-Mar) and summer months (Jun-Sept) suggesting other drivers of daily changes in groundwater levels. Similarly, the relationship between transpiration and water table height remained weak ($r \leq 0.5$) throughout much of the growing season. Notably, unlike previous work in locations where transpiration drove diel fluxes, there was no clear pattern in correlation with increasing lag as the summer progressed and subsurface layers dried (Bond et al., 2002; Graham et al., 2010). Though it remains unclear as to what is driving the observed diel fluctuations, we take the poor relationship between groundwater levels and transpiration to suggest trees are not sourcing moisture directly from the saturated zone, further indicating rock moisture is a crucial source of tree available water.

Reductions in Rock Moisture Mirrors Vegetation Density and Subsurface Structure:

Observed reductions in rock moisture mirrored aboveground forest densities and measured transpiration rates. For example, 19 mm and 30 mm of dynamic rock moisture were measured by NMR surveys in the Cut-Plot-N and Upper-S boreholes, respectively. These values, roughly 70 and 53 % less than what was observed at the Mid-S plot, correspond with a >95 and 47 % difference in basal area. Similarly, comparisons among locations with both sapflow and rock-moisture measurements showed increased rock moisture reductions where transpiration was

greater. Total transpired amounts and rock moisture reductions at the Mid-S plot were 24 % and 22 % greater respectively than at the Lower-S plot. Other factors that might lead to variable water use between plots further support the pairing of transpiration and rock moisture extraction. Soil moisture was lower at the Mid-S plot while shallow seismic surveys by Befus et al (2011) and fracture density counts by St. Clair et al. (2015) indicate similar weathering depths and fracture densities at both locations.

Vertical distribution of dynamic rock moisture within a borehole corresponded with subsurface structure. Previous seismic work in the uppermost portion of Gordon Gulch imaged unweathered rock at 15 m depth (Befus et al., 2011). Intermediate velocity material extended to 4 m deep with <2 m of low velocity on both slopes. Though the Befus et al. (2011) velocities assigned to soil and mobile regolith suggest deeper soils than we found while installing soil sensors or what has been observed in pits (Anderson et al., 2021), their total depth of low- and intermediate-velocity materials correspond with the depth of dynamic rock moisture. Across the catena of hillslopes, the greatest changes in rock moisture occurred below the soil-saprolite interface and 2 m depth. No changes in rock moisture were observed below 5 m in any borehole.

This pattern of dynamic rock moisture being confined to depths with lower or intermediate seismic velocities could be important for our understanding of water availability within Gordon Gulch and elsewhere. For example, while some models and geophysical data have suggested weathering is generally deeper on north- versus south-facing slopes, indicating potentially greater storage (Anderson et al., 2013; Befus et al., 2011), others have found contradictory evidence suggesting saprolite is either thicker on southern aspects or shows little variation between aspects (Bandler,

2015; St. Clair et al., 2015). As our results show dynamic rock moisture is limited to depths between the soil and 5 m or largely the saprolite layer, resolving these discrepancies in our understanding of weathering depth will be critical in determining potential water availability.

Uptake of Rock Moisture May Mitigate Onset of Drought-Stress:

The uptake of rock moisture may mediate drought stress in upper montane tree species when soil moisture is limited. Increases in estimated root PLC corresponded with the greatest reductions in rock moisture at both south-facing plots. Previous work has shown mature ponderosa pine and Douglas-fir trees are capable of significant hydraulic lift and redistribution (Brooks et al., 2002). Others have shown hydraulic redistribution can vary by nearly two orders of magnitude, with ponderosa pine values ranging from 0.2 to 1.0 mm d⁻¹ (Neumann and Cardon, 2012). Domec et al. (2004) showed ponderosa pine and Douglas-fir trees limit loss of shallow root function through hydraulic redistribution. Though we have no direct evidence of hydrologic redistribution at our site (i.e. daily fluctuations in soil moisture were within the margin of error for soil moisture sensors), our transpiration measurements indicated that the trees remained responsive to late-season summer rains even after estimated PLC exceeded 60%, suggesting roots at shallow depths were potentially highly or fully compromised. Although calculated PLC values can be much more negative than those measured in the field (Domec et al., 2004), the rapid response of transpiration to small increases in shallow soil moisture suggests that the shallow root conducting system was being maintained by sources of water beyond the bulk soil matrix. We speculate that hydraulic redistribution of water maintained shallow root conductivity and preserved some shallow root function (Domec et al., 2004). Through repeated electrical resistivity surveys, Mares et al. (2016) suggested potential hydraulic redistribution on the south-facing slope in the lower elevation

portion of Gordon Gulch. Though our data are limited to just two plots on the south-facing slope where deep boreholes, transpiration, and soil moisture were co-located, our results suggest rock moisture may be a source of deeper water that can be redistributed to shallow depths to maintain shallow root function.

Implications of Rock Moisture:

While plant use of rock moisture is becoming well-documented in rain-dominated environments, and recent work has shown rock moisture use to be widespread and routine (Hahm, Dralle, et al., 2019; Hahm et al., 2020; McCormick et al., 2021; Rempe and Dietrich, 2018), understanding rock moisture storage and use in snow-dominated montane catchments is of particular societal and ecological importance. Snow-dominated montane catchments are critical sources of water for human use (Bales et al., 2006; Mote et al., 2005), serve as an important carbon sink (Pacala et al., 2001; Schimel et al., 2002), and are home to millions of people living in the wildland-urban interface (Theobald and Romme, 2007). These ecosystems are also among the most vulnerable to anthropogenic climate change (Beniston, 2003; Millar et al., 2007).

As temperatures warm and snowpack declines, rock moisture storage may directly impact tree mortality and resiliency, particularly as systems move from energy-limited to water-limited. For example, during the 2011–2016 drought in California, where high temperatures and low precipitation led to widespread tree die off, variations in storage led to diverse and sometimes counterintuitive responses. Goulden and Bales (2019) found that in areas where storage was greater than precipitation, deep subsurface storage led to water stress during consecutive drought years because storage was not replenished by precipitations. In these instances, wet years filled

substantial subsurface storage beyond yearly transpiration levels. This excess storage then supplied the necessary water for structural overshoot or growth beyond what could normally be supported in an average water year. However, when multiple dry and hot years persisted subsurface reservoirs became successively drier and the structural overshoot that occurred during wet years amplified drying by increasing tree water demand. Hahm et al. (2019) reported similar patterns, labeling these ecosystems, “precipitation limited.”

Hahm et al. (2019) also showed that in “storage limited” locations, where rock and soil storage capacity is less than annual precipitation, rock moisture can mitigate drought stress. In these locations, subsurface reservoirs are filled each year to the same level regardless of wet or dry year status. Thus, trees in these areas experience the same level of stress each year and are “decoupled” from annual precipitation. While more than 100 million trees died across California in the 2011-2016 drought (USFS, 2016), Hahm et al. (2019) found no significant tree mortality at sites storage was similar across years experiencing a large range in rainfall totals. In contrast, where storage capacity is large relative to annual rainfall totals, Hahm et al., (2019) posited that trees would be strongly sensitive to the precipitation totals and vulnerable to drought. Though our study only spanned one growing season and is therefore unable to elucidate multi-year patterns, it is likely that similar storage-precipitation relationships exist at our snow dominated site. Further work, across greater spatial and temporal scales is needed to clarify the role of rock moisture storage and use under present and future temperature and precipitation regimes.

CONCLUSIONS

This study documents growing season moisture sources to a mixed conifer forest within north- and south-facing hillslope aspects in the Rocky Mountains. Soils supply moisture during wet periods following snowmelt and summer rainfall events, and rock moisture supports late dry-season transpiration. Groundwater is likely too deep to support vegetation across much of the study area. Even in the wetter than average year, transpiration that occurs during the late dry season is likely sourced from rock moisture. The timing of directly observed rock moisture depletion suggests that rock moisture is lost to transpiration rather than vertical drainage. This study highlights the significance of rock moisture storage dynamics in snow-dominated catchments and supports previous work suggesting that rock moisture is central to water cycling in uplands regions. Further work across greater spatial and temporal scales is needed to accurately incorporate the implications of dynamic rock moisture into future predictions and management of upper montane forests.

BIBLIOGRAPHY

- Adams, H. D., Zeppel, M. J. B., Anderegg, W. R. L., Hartmann, H., Landhäusser, S. M., Tissue, D. T., et al. (2017). A multi-species synthesis of physiological mechanisms in drought-induced tree mortality. *Nature Ecology and Evolution*, 1(9), 1285–1291. <https://doi.org/10.1038/s41559-017-0248-x>
- Alton, P., Fisher, R., Los, S., and Williams, M. (2009). Simulations of global evapotranspiration using semiempirical and mechanistic schemes of plant hydrology. *Global Biogeochemical Cycles*, 23(4). <https://doi.org/10.1029/2009GB003540>
- Ameglio, T., Archer, P., Cohen, M., Valancogne, C., Dayau, S., and Cruiziat, P. (n.d.). Significance and limits in the use of predawn leaf water potential for tree irrigation, 13.
- Anderson, R. S., Anderson, S. P., and Tucker, G. E. (2013). Rock damage and regolith transport by frost: an example of climate modulation of the geomorphology of the critical zone. *Earth Surface Processes and Landforms*, 38(3), 299–316. <https://doi.org/10.1002/esp.3330>
- Anderson, S. P., Kelly, P. J., Hoffman, N., Barnhart, K., Befus, K., and Ouimet, W. (2021). Is This Steady State? Weathering and Critical Zone Architecture in Gordon Gulch, Colorado Front Range. In A. Hunt, M. Egli, and B. Faybishenko (Eds.), *Geophysical Monograph Series* (1st ed., pp. 231–252). Wiley. <https://doi.org/10.1002/9781119563952.ch13>
- Bales, R. C., Molotch, N. P., Painter, T. H., Dettinger, M. D., Rice, R., and Dozier, J. (2006). Mountain hydrology of the western United States. *Water Resources Research*, 42(8). <https://doi.org/10.1029/2005WR004387>
- Bandler, A. J. (2015, December 31). Geophysical constraints on critical zone architecture and subsurface hydrology of opposing montane hillslopes (Text). Colorado School of Mines. Retrieved from <http://mountainscholar.org/handle/11124/170251>
- Barnard, H. R., Graham, C. B., Van Verseveld, W. J., Brooks, J. R., Bond, B. J., and McDonnell, J. J. (2010). Mechanistic assessment of hillslope transpiration controls of diel subsurface flow: a steady-state irrigation approach. *Ecohydrology*, 3(2), 133–142. <https://doi.org/10.1002/eco.114>
- Barrett, D. J., Hatton, T. J., Ash, J. E., and Ball, M. C. (1995). Evaluation of the heat pulse velocity technique for measurement of sap flow in rainforest and eucalypt forest species of south-eastern Australia. *Plant, Cell and Environment*, 18(4), 463–469. <https://doi.org/10.1111/j.1365-3040.1995.tb00381.x>
- Befus, K. M., Sheehan, A. F., Leopold, M., Anderson, S. P., and Anderson, R. S. (2011). Seismic Constraints on Critical Zone Architecture, Boulder Creek Watershed, Front Range, Colorado. *Vadose Zone Journal*, 10(3), 915–927. <https://doi.org/10.2136/vzj2010.0108>

- Bell, J. P. (1987). Neutron probe practice. 3rd edition. [Publication - Report]. Retrieved April 25, 2022, from <http://nora.nerc.ac.uk/id/eprint/5629/>
- Beniston, M. (2003). Climatic Change in Mountain Regions: A Review of Possible Impacts. *Climatic Change*, 59(1), 5–31. <https://doi.org/10.1023/A:1024458411589>
- Berghuijs, W. R., Woods, R. A., and Hrachowitz, M. (2014). A precipitation shift from snow towards rain leads to a decrease in streamflow. *Nature Climate Change*, 4(7), 583–586. <https://doi.org/10.1038/nclimate2246>
- Bond, B. J., Jones, J. A., Moore, G., Phillips, N., Post, D., and McDonnell, J. J. (2002). The zone of vegetation influence on baseflow revealed by diel patterns of streamflow and vegetation water use in a headwater basin. *Hydrological Processes*, 16(8), 1671–1677. <https://doi.org/10.1002/hyp.5022>
- Brantley, S. L., Eissenstat, D. M., Link to external site, this link will open in a new window, Marshall, J. A., Link to external site, this link will open in a new window, Godsey, S. E., et al. (2017). Reviews and syntheses: on the roles trees play in building and plumbing the critical zone. *Biogeosciences; Katlenburg-Lindau*, 14(22), 5115–5142. <http://dx.doi.org.colorado.idm.oclc.org/10.5194/bg-14-5115-2017>
- Brooks, J. R., Meinzer, F. C., Coulombe, R., and Gregg, J. (2002). Hydraulic redistribution of soil water during summer drought in two contrasting Pacific Northwest coniferous forests. *Tree Physiology*, 22(15–16), 1107–1117. <https://doi.org/10.1093/treephys/22.15-16.1107>
- Brooks, P. D., Chorover, J., Fan, Y., Godsey, S. E., Maxwell, R. M., McNamara, J. P., and Tague, C. (2015). Hydrological partitioning in the critical zone: Recent advances and opportunities for developing transferable understanding of water cycle dynamics. *Water Resources Research*, 51(9), 6973–6987. <https://doi.org/10.1002/2015WR017039>
- Burgess, S. S. O., Adams, M. A., Turner, N. C., Beverly, C. R., Ong, C. K., Khan, A. A. H., and Bleby, T. M. (2001). An improved heat pulse method to measure low and reverse rates of sap flow in woody plants. *Tree Physiology*, 21(9), 589–598. <https://doi.org/10.1093/treephys/21.9.589>
- Canadell, J., Jackson, R. B., Ehleringer, J. B., Mooney, H. A., Sala, O. E., and Schulze, E.-D. (1996). Maximum rooting depth of vegetation types at the global scale. *Oecologia*, 108(4), 583–595. <https://doi.org/10.1007/BF00329030>
- Clair, J. S., Moon, S., Holbrook, W. S., Perron, J. T., Riebe, C. S., Martel, S. J., et al. (2015). Geophysical imaging reveals topographic stress control of bedrock weathering. *Science*, 350(6260), 534–538. <https://doi.org/10.1126/science.aab2210>
- Crifasi, R. R. (2015). A Land Made from Water: Appropriation and the Evolution of Colorado's Landscape, Ditches, and Water Institutions. Colorado, UNITED STATES: University

Press of Colorado. Retrieved from
<http://ebookcentral.proquest.com/lib/ucb/detail.action?docID=4415136>

- Diek, S., Temme, A. J. A. M., and Teuling, A. (2013, April 1). Assessing the effect of soil diversity on the hydrology of a complex landscape - a case study in Gordon Gulch Valley, Colorado Front Range of the Rocky Mountains.
- Domec, J.-C., Warren, J. M., Meinzer, F. C., Brooks, J. R., and Coulombe, R. (2004). Native root xylem embolism and stomatal closure in stands of Douglas-fir and ponderosa pine: mitigation by hydraulic redistribution. *Oecologia*, 141(1), 7–16.
<https://doi.org/10.1007/s00442-004-1621-4>
- Earman, S., Campbell, A. R., Phillips, F. M., and Newman, B. D. (2006). Isotopic exchange between snow and atmospheric water vapor: Estimation of the snowmelt component of groundwater recharge in the southwestern United States. *Journal of Geophysical Research: Atmospheres*, 111(D9). <https://doi.org/10.1029/2005JD006470>
- Gardner, W. H. (1986). Water content. *Methods of Soil Analysis: Part 1* (2nd ed., Vol. 5).
Godsey, S. E., Kirchner, J. W., and Tague, C. L. (2014). Effects of changes in winter snowpacks on summer low flows: case studies in the Sierra Nevada, California, USA. *Hydrological Processes*, 28(19), 5048–5064. <https://doi.org/10.1002/hyp.9943>
- Goldblum, D., and Veblen, T. T. (2013). FIRE HISTORY OF A PONDEROSA PINE/DOUGLAS FIR FOREST IN THE COLORADO FRONT RANGE. *Physical Geography*. Retrieved from
<http://www.tandfonline.com/doi/abs/10.1080/02723646.1992.10642449>
- Goulden, M. L., and Bales, R. C. (2019). California forest die-off linked to multi-year deep soil drying in 2012–2015 drought. *Nature Geoscience*, 12(8), 632–637.
<https://doi.org/10.1038/s41561-019-0388-5>
- Graham, C. B., van Verseveld, W., Barnard, H. R., and McDonnell, J. J. (2010). Estimating the deep seepage component of the hillslope and catchment water balance within a measurement uncertainty framework. *Hydrological Processes*, 24(25), 3631–3647.
<https://doi.org/10.1002/hyp.7788>
- Gribovszki, Z., Szilágyi, J., and Kalicz, P. (2010). Diurnal fluctuations in shallow groundwater levels and streamflow rates and their interpretation – A review. *Journal of Hydrology*, 385(1–4), 371–383. <https://doi.org/10.1016/j.jhydrol.2010.02.001>
- Hahm, W. J., Rempe, D. M., Dralle, D. N., Dawson, T. E., Lovill, S. M., Bryk, A. B., et al. (2019). Lithologically Controlled Subsurface Critical Zone Thickness and Water Storage Capacity Determine Regional Plant Community Composition. *Water Resources Research*, 55(4), 3028–3055. <https://doi.org/10.1029/2018WR023760>

- Hahm, W. J., Dralle, D. N., Rempe, D. M., Bryk, A. B., Thompson, S. E., Dawson, T. E., and Dietrich, W. E. (2019). Low Subsurface Water Storage Capacity Relative to Annual Rainfall Decouples Mediterranean Plant Productivity and Water Use From Rainfall Variability. *Geophysical Research Letters*, 46(12), 6544–6553. <https://doi.org/10.1029/2019GL083294>
- Hahm, W. J., Rempe, D. M., Dralle, D. N., Dawson, T. E., and Dietrich, W. E. (2020). Oak Transpiration Drawn From the Weathered Bedrock Vadose Zone in the Summer Dry Season. *Water Resources Research*, 56(11). <https://doi.org/10.1029/2020WR027419>
- Hammond, W. M., Yu, K., Wilson, L. A., Will, R. E., Anderegg, W. R. L., and Adams, H. D. (2019). Dead or dying? Quantifying the point of no return from hydraulic failure in drought-induced tree mortality. *New Phytologist*, 223(4), 1834–1843. <https://doi.org/10.1111/nph.15922>
- Harmon, R., Barnard, H. R., and Singha, K. (2020). Water Table Depth and Bedrock Permeability Control Magnitude and Timing of Transpiration-Induced Diel Fluctuations in Groundwater. *Water Resources Research*, 56(5), e2019WR025967. <https://doi.org/10.1029/2019WR025967>
- Harpold, A., Brooks, P., Rajagopal, S., Heidebuchel, I., Jardine, A., and Stielstra, C. (2012). Changes in snowpack accumulation and ablation in the intermountain west. *Water Resources Research*, 48(11). <https://doi.org/10.1029/2012WR011949>
- Hellmers, H., Horton, J. S., Juhren, G., and O’Keefe, J. (1955). Root Systems of Some Chaparral Plants in Southern California. *Ecology*, 36(4), 667–678. <https://doi.org/10.2307/1931305>
- Hinckley, E.-L. S., Ebel, B. A., Barnes, R. T., Anderson, R. S., Williams, M. W., and Anderson, S. P. (2014). Aspect control of water movement on hillslopes near the rain–snow transition of the Colorado Front Range. *Hydrological Processes*, 28(1), 74–85. <https://doi.org/10.1002/hyp.9549>
- Hu, J., Moore, D. J. P., Burns, S. P., and Monson, R. K. (2010). Longer growing seasons lead to less carbon sequestration by a subalpine forest. *Global Change Biology*, 16(2), 771–783. <https://doi.org/10.1111/j.1365-2486.2009.01967.x>
- Jasechko, S., Sharp, Z. D., Gibson, J. J., Birks, S. J., Yi, Y., and Fawcett, P. J. (2013). Terrestrial water fluxes dominated by transpiration. *Nature*, 496(7445), 347–350. <https://doi.org/10.1038/nature11983>
- Klos, P. Z., Goulden, M. L., Riebe, C. S., Tague, C. L., O’Geen, A. T., Flinchum, B. A., et al. (2018). Subsurface plant-accessible water in mountain ecosystems with a Mediterranean climate. *WIREs Water*, 5(3), e1277. <https://doi.org/10.1002/wat2.1277>
- Kramer, P. J. and Boyer, J. S. (1995). *Water Relation of Plants and Soils*. London: Academic Press.

- Kurpius, M. R., Panek, J. A., Nikolov, N. T., McKay, M., and Goldstein, A. H. (2003). Partitioning of water flux in a Sierra Nevada ponderosa pine plantation. *Agricultural and Forest Meteorology*, 117(3–4), 173–192. [https://doi.org/10.1016/S0168-1923\(03\)00062-5](https://doi.org/10.1016/S0168-1923(03)00062-5)
- Leopold, M., Völkel, J., Huber, J., and Dethier, D. (2013). Subsurface architecture of the Boulder Creek Critical Zone Observatory from electrical resistivity tomography. *Earth Surface Processes and Landforms*, 38(12), 1417–1431. <https://doi.org/10.1002/esp.3420>
- Lewis, D. C., and Burgy, R. H. (1964). The Relationship between oak tree roots and groundwater in fractured rock as determined by tritium tracing. *Journal of Geophysical Research (1896-1977)*, 69(12), 2579–2588. <https://doi.org/10.1029/JZ069i012p02579>
- Li, X., Gentine, P., Lin, C., Zhou, S., Sun, Z., Zheng, Y., et al. (2019). A simple and objective method to partition evapotranspiration into transpiration and evaporation at eddy-covariance sites. *Agricultural and Forest Meteorology*, 265, 171–182. <https://doi.org/10.1016/j.agrformet.2018.11.017>
- Mares, R., Barnard, H. R., Mao, D., Revil, A., and Singha, K. (2016). Examining diel patterns of soil and xylem moisture using electrical resistivity imaging. *Journal of Hydrology*, 536, 327–338. <https://doi.org/10.1016/j.jhydrol.2016.03.003>
- Marshall, D. C. (1958). Measurement of Sap Flow in Conifers by Heat Transport. 1. Plant Physiology, 33(6), 385–396. <https://doi.org/10.1104/pp.33.6.385>
- McCormick, E. L., Dralle, D. N., Hahm, W. J., Tune, A. K., Schmidt, L. M., Chadwick, K. D., and Rempe, D. M. (2021). Widespread woody plant use of water stored in bedrock. *Nature*, 597(7875), 225–229. <https://doi.org/10.1038/s41586-021-03761-3>
- McDowell, N. G., Grossiord, C., Adams, H. D., Pinzón-Navarro, S., Mackay, D. S., Breshears, D. D., et al. (2019). Mechanisms of a coniferous woodland persistence under drought and heat. *Environmental Research Letters*, 14(4), 045014. <https://doi.org/10.1088/1748-9326/ab0921>
- Millar, C. I., Stephenson, N. L., and Stephens, S. L. (2007). Climate Change and Forests of the Future: Managing in the Face of Uncertainty. *Ecological Applications*, 17(8), 2145–2151. <https://doi.org/10.1890/06-1715.1>
- Moore, J. (n.d.). 2016 Aerial Survey Results: California, 18.
- Mote, P. W., Hamlet, A. F., Clark, M. P., and Lettenmaier, D. P. (2005). DECLINING MOUNTAIN SNOWPACK IN WESTERN NORTH AMERICA*. *Bulletin of the American Meteorological Society*, 86(1), 39–50. <https://doi.org/10.1175/BAMS-86-1-39>

- Mote, P. W., Li, S., Lettenmaier, D. P., Xiao, M., and Engel, R. (2018). Dramatic declines in snowpack in the western US. *Npj Climate and Atmospheric Science*, 1(1), 1–6. <https://doi.org/10.1038/s41612-018-0012-1>
- Neumann, R. B., and Cardon, Z. G. (2012). The magnitude of hydraulic redistribution by plant roots: a review and synthesis of empirical and modeling studies. *New Phytologist*, 194(2), 337–352. <https://doi.org/10.1111/j.1469-8137.2012.04088.x>
- Pacala, S. W., Hurtt, G. C., Baker, D., Peylin, P., Houghton, R. A., Birdsey, R. A., et al. (2001). Consistent Land- and Atmosphere-Based U.S. Carbon Sink Estimates. *Science*. <https://doi.org/10.1126/science.1057320>
- Pataki, D. E., Oren, R., and Smith, W. K. (2000). Sap Flux of Co-Occurring Species in a Western Subalpine Forest during Seasonal Soil Drought. *Ecology*, 81(9), 2557–2566. <https://doi.org/10.2307/177474>
- Piñol, J., and Sala, A. (2000). Ecological implications of xylem cavitation for several Pinaceae in the Pacific Northern USA. *Functional Ecology*, 14(5), 538–545. <https://doi.org/10.1046/j.1365-2435.2000.t01-1-00451.x>
- Rempe, D. M., and Dietrich, W. E. (2014). A bottom-up control on fresh-bedrock topography under landscapes. *Proceedings of the National Academy of Sciences*, 111(18), 6576–6581. <https://doi.org/10.1073/pnas.1404763111>
- Rempe, D. M., and Dietrich, W. E. (2018). Direct observations of rock moisture, a hidden component of the hydrologic cycle. *Proceedings of the National Academy of Sciences*, 115(11), 2664–2669. <https://doi.org/10.1073/pnas.1800141115>
- Rose, K., Graham, R., and Parker, D. (2003). Water source utilization by *Pinus jeffreyi* and *Arctostaphylos patula* on thin soils over bedrock. *Oecologia*, 134(1), 46–54. <https://doi.org/10.1007/s00442-002-1084-4>
- Salve, R., Rempe, D. M., and Dietrich, W. E. (2012). Rain, rock moisture dynamics, and the rapid response of perched groundwater in weathered, fractured argillite underlying a steep hillslope. *Water Resources Research*, 48(11). <https://doi.org/10.1029/2012WR012583>
- Schenk, H. J., and Jackson, R. B. (2002). The Global Biogeography of Roots. *Ecological Monographs*, 72(3), 311–328. [https://doi.org/10.1890/0012-9615\(2002\)072\[0311:TGBOR\]2.0.CO;2](https://doi.org/10.1890/0012-9615(2002)072[0311:TGBOR]2.0.CO;2)
- Schimel, D., Kittel, T. G. F., Running, S., Monson, R., Turnipseed, A., and Anderson, D. (2002). Carbon sequestration studied in western U.S. mountains. *Eos, Transactions American Geophysical Union*, 83(40), 445–449. <https://doi.org/10.1029/2002EO000314>

- Seyfried, M. S., Murdock, M. D., Hanson, C. L., Flerchinger, G. N., and Vactor, S. V. (2001). Long-Term Soil Water Content Database, Reynolds Creek Experimental Watershed, Idaho, United States. Retrieved from <https://pubag.nal.usda.gov/catalog/60521>
- Steppe, K., Pauw, D. J. W. de, Doody, T. M., and Teskey, R. O. (2010). A comparison of sap flux density using thermal dissipation, heat pulse velocity and heat field deformation methods. *Agricultural and Forest Meteorology*, 150(7/8), 1046–1056.
- Stone, E. L., and Kalisz, P. J. (1991). On the maximum extent of tree roots. *Forest Ecology and Management*, 46(1–2), 59–102. [https://doi.org/10.1016/0378-1127\(91\)90245-Q](https://doi.org/10.1016/0378-1127(91)90245-Q)
- Sucoff, E. (1972). Water Potential in Red Pine: Soil Moisture, Evapotranspiration, Crown Position. *Ecology*, 53(4), 681–686. <https://doi.org/10.2307/1934783>
- Theobald, D. M., and Romme, W. H. (2007). Expansion of the US wildland–urban interface. *Landscape and Urban Planning*, 83(4), 340–354. <https://doi.org/10.1016/j.landurbplan.2007.06.002>
- Trujillo, E., Molotch, N. P., Goulden, M. L., Kelly, A. E., and Bales, R. C. (2012). Elevation-dependent influence of snow accumulation on forest greening. *Nature Geoscience*, 5(10), 705–709. <https://doi.org/10.1038/ngeo1571>
- Wald, J., Graham, R., and Schoeneberger, P. (2013). Distribution and properties of soft weathered bedrock at ≤ 1 m depth in the contiguous United States. *Earth Surface Processes and Landforms*, 38, 614–626. <https://doi.org/10.1002/esp.3343>
- Walsh, D., Turner, P., Grunewald, E., Zhang, H., Butler Jr., J. J., Reboulet, E., et al. (2013). A Small-Diameter NMR Logging Tool for Groundwater Investigations. *Groundwater*, 51(6), 914–926. <https://doi.org/10.1111/gwat.12024>
- Warrell, K. F. (2011). Stream Terraces in the Critical Zone - Lower Gordon Gulch, Colorado. (Masters thesis). Georgia Institute of Technology, Atlanta, GA. <http://hdl.handle.net/1853/38839>
- White. (1932). A method of estimating ground-water supplies based on discharge by plants and evaporation from soil: Results of investigations in Escalante Valley, Utah. <https://doi.org/10.3133/wsp659A>
- Williams, J., and Sinclair, D. F. (1981). Accuracy, bias and precision. Australia: CSIRO.
- Zwieniecki, M. A., and Newton, M. (1996). Water-Holding Characteristics of Metasedimentary Rock in Selected Forest Ecosystems in Southwestern Oregon. *Soil Science Society of America Journal*, 60(5), 1578–1582. <https://doi.org/10.2136/sssaj1996.03615995006000050042x>

SUPPLEMENTAL TABLES and FIGURES

Table S1: NMR and neutron probe survey dates

NMR and Neutron Probe Surveys		
Date	NMR	Neutron Probe
5/20/21	x	
6/2/21	x	
6/22/21	x	
7/26/21	x	x
8/3/21		x
8/10/21		x
8/17/21	x	x
8/24/21		x
8/31/21		x
9/27/21	x	x

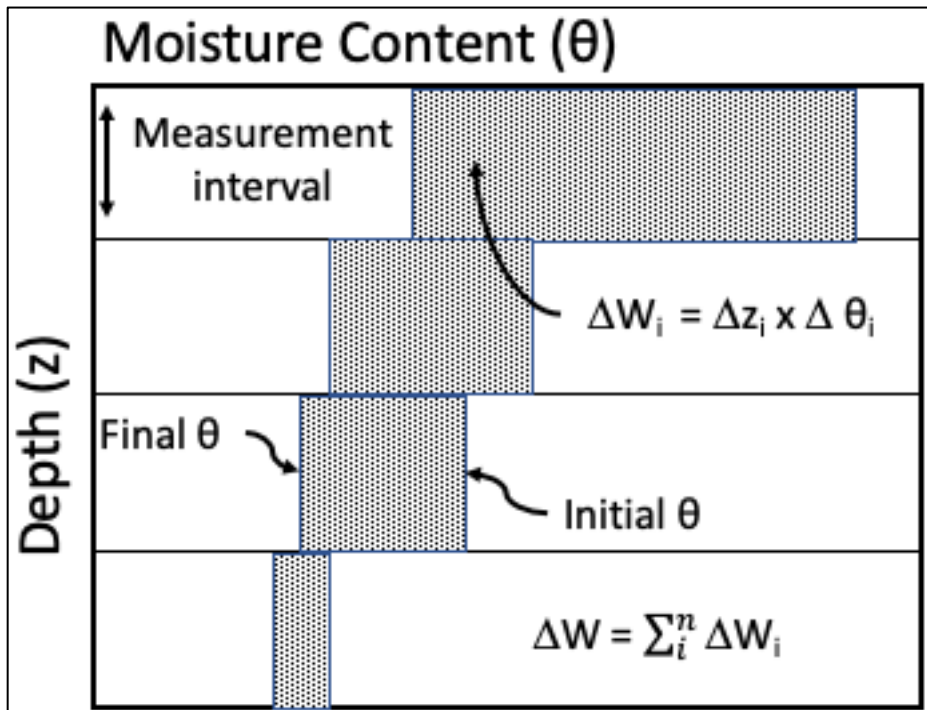
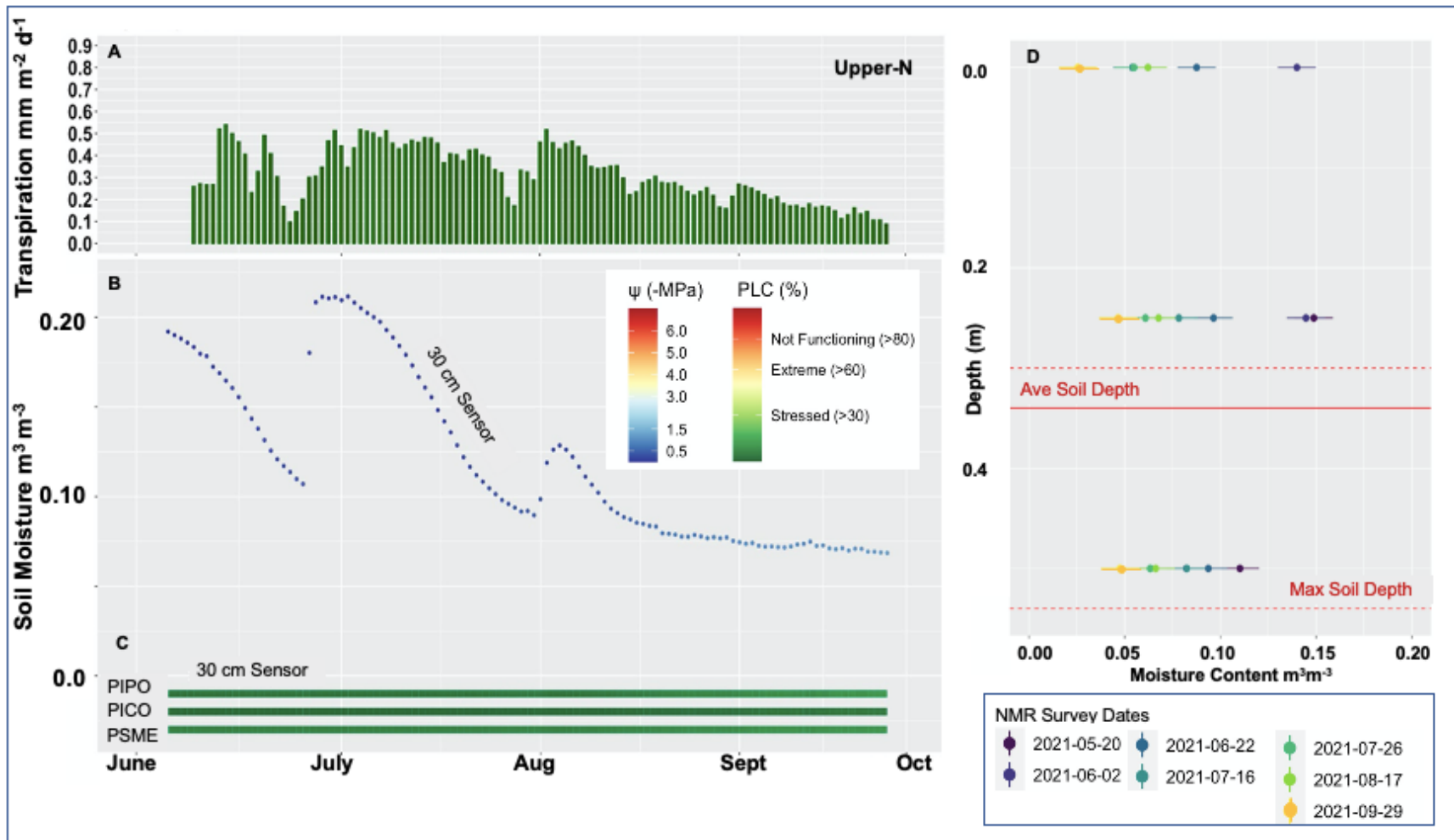
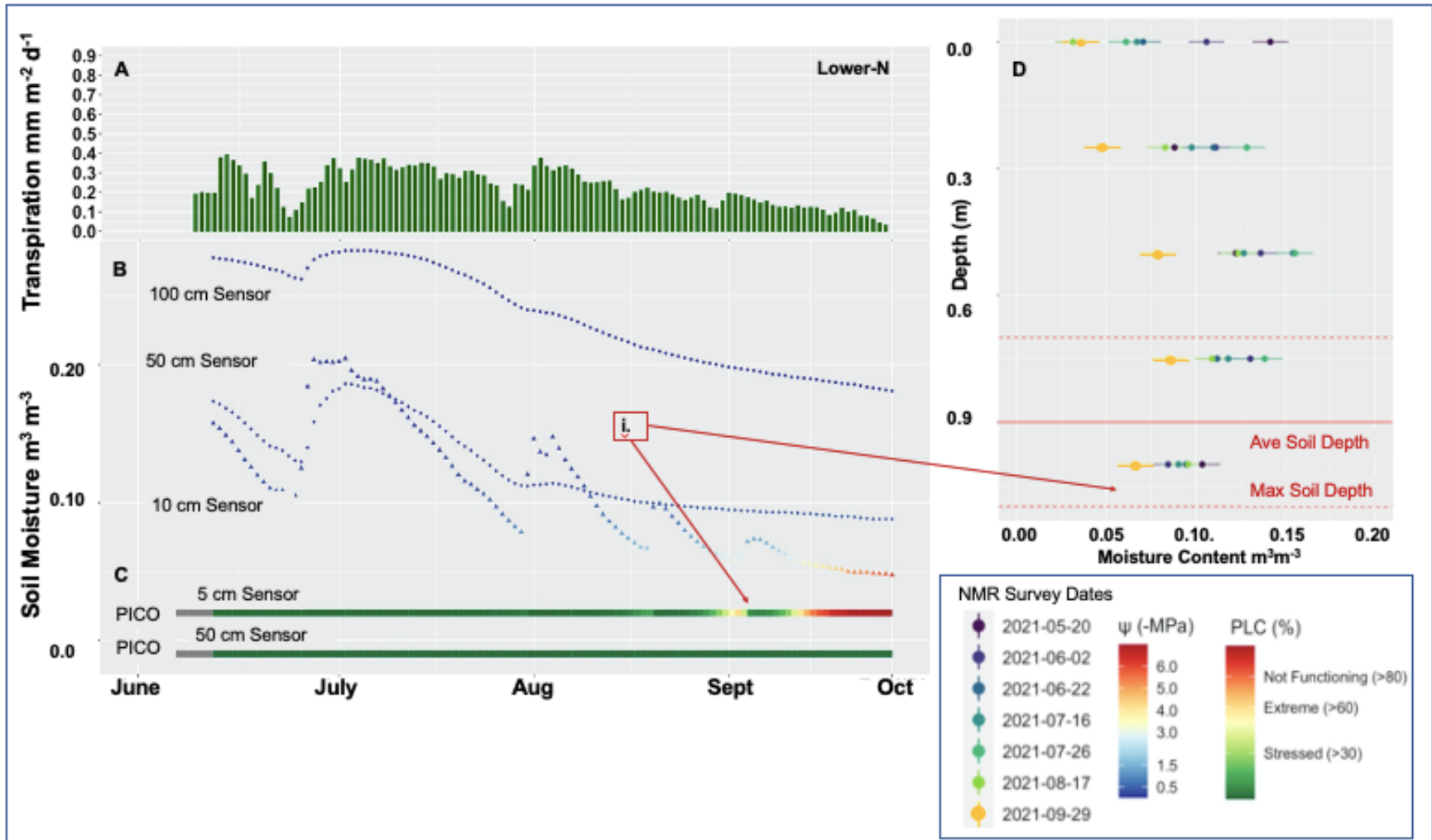


Figure S1: Schematic showing how dynamic rock moisture ($S_{dynamic}$) is calculated. Assuming water content is the same over a given depth interval, the change in water content at a given interval (ΔW_i) is equal to the depth of that interval multiplied by the change in water content measured for that depth interval. The total change in water content of the borehole (ΔW) is the sum of all ΔW_i .



Figures S2: A Plot level transpiration. B) Soil moisture with calculated matric potential overlaid in blue to red. C) Calculated PLC values in green to red bars. D) Change in rock moisture sense wettest survey on May 20th for given depths. Malfunctioning sensor at 10cm limits insight into soil moisture content. NMR surveys in soil column (upper portion of panel D) show gradual drying similar to lower north-facing plot



Figures S3: A) Plot level transpiration. B) Soil moisture with calculated matric potential overlaid in blue to red. C) Calculated PLC values in green to red bars. D) Change in rock moisture sense wettest survey on May 20th for given depths. i) Measurable changes in moisture at soil-saprolite interface only occur as roots in shallow soil become stressed.

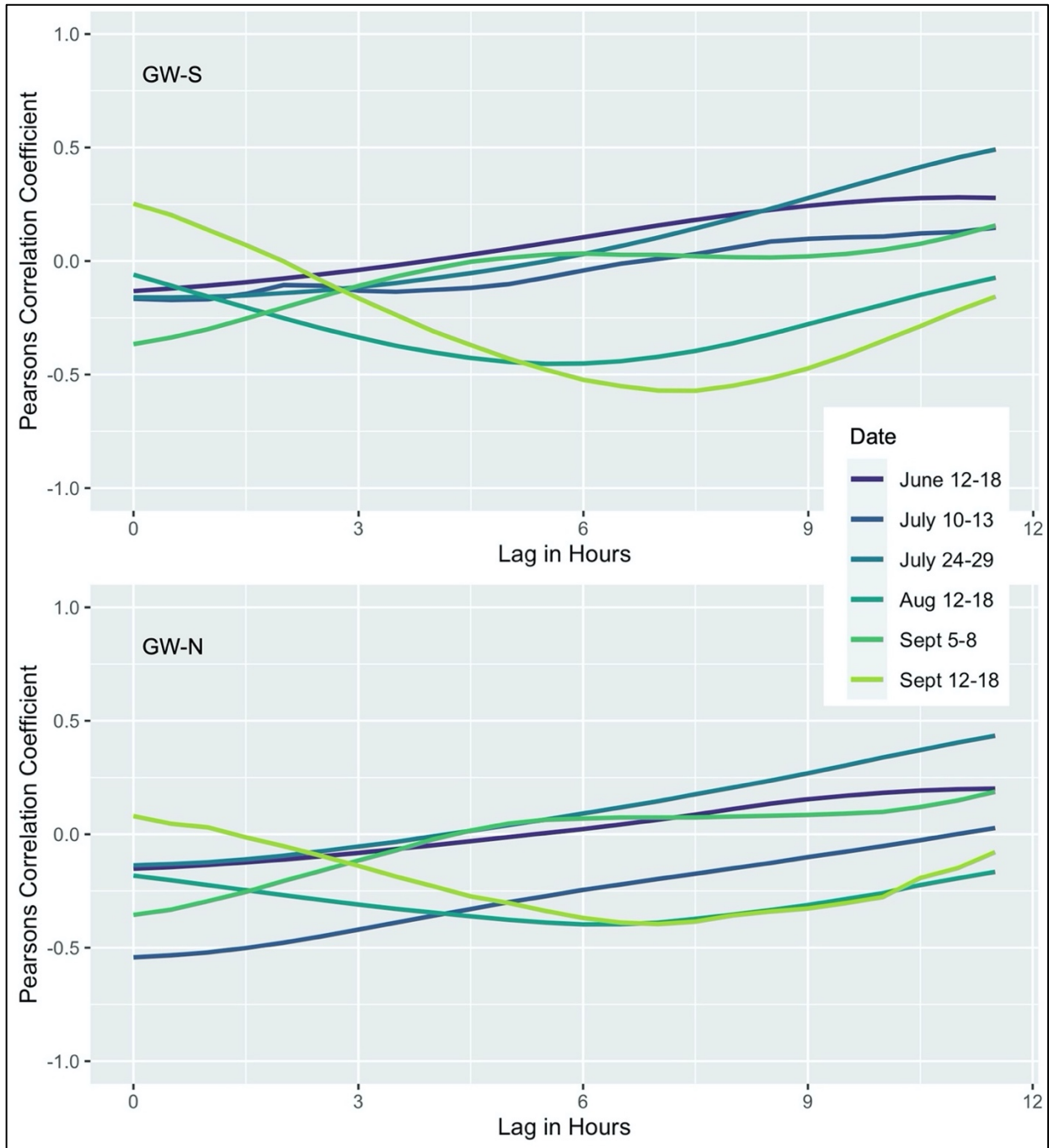


Figure S4: Correlation between transpiration and groundwater for the south facing groundwater well (GW-S) and the north facing groundwater well (GW-N). Both show only moderate to poor correlation with no pattern of increased lag as the subsurface dries.

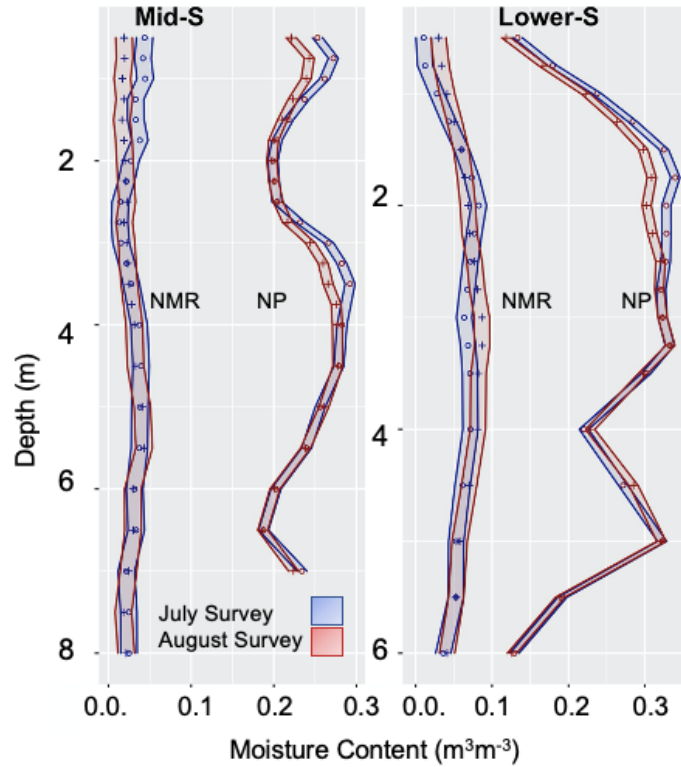


Figure S5: Side by side comparisons of NMR and neutron probe surveys completed on the same dates. Neutron probe surveys are on the right of each panel and have lower associated error and show that changes in moisture content (m^3m^{-3}) as measured by NMR are conservative estimates. However, the two methods show similar depth of dynamic moisture and the same directional change in moisture content.